JEM Journal of Experimental Medicine

TECHNICAL ADVANCES AND RESOURCES

Human IgA binds a diverse array of commensal bacteria

Delphine Sterlin[1*], Jehane Fadlallah[1*], Olivia Adams[2*], Claire Fieschi[3], Christophe Parizot[1], Karim Dorgham[1], Asok Rajkumar[1], Gaëlle Autaa[1], Hela El-Kafsi[1], Jean-Luc Charuel[1], Catherine Juste[4], Friederike Jönsson[5], Thomas Candela[6], Hedda Wardemann[7], Alexandra Aubry[1], Carmen Capito[6], Hélène Brisson[1], Christophe Tresallet[8], Richard D. Cummings[9], Martin Larsen[1], Hans Yssel[1], Stephan von Gunten[2], and Guy Gorochov[1]

In humans, several grams of IgA are secreted every day in the intestinal lumen. While only one IgA isotype exists in mice, humans secrete IgA1 and IgA2, whose respective relations with the microbiota remain elusive. We compared the binding patterns of both polyclonal IgA subclasses to commensals and glycan arrays and determined the reactivity profile of native human monoclonal IgA antibodies. While most commensals are dually targeted by IgA1 and IgA2 in the small intestine, IgA1$^+$IgA2$^+$ and IgA1$^-$IgA2$^+$ bacteria coexist in the colon lumen, where Bacteroidetes is preferentially targeted by IgA2. We also observed that galactose-α terminated glycans are almost exclusively recognized by IgA2. Although bearing signs of affinity maturation, gut-derived IgA monoclonal antibodies are cross-reactive in the sense that they bind to multiple bacterial targets. Private anticarbohydrate-binding patterns, observed at clonal level as well, could explain these apparently opposing features of IgA, being at the same time cross-reactive and selective in its interactions with the microbiota.

Introduction

IgA is the second most important isotype in serum, with secretory IgA being predominant in gut lumen, where its functions range from host-commensal symbiosis to protection against enteric pathogens. IgA contributes to intestinal homeostasis, either by directly inhibiting bacterial virulence features or by shaping microbiota composition and promoting symbiosis between bacteria (Forbes et al., 2008, 2011; Okai et al., 2016; Nakajima et al., 2018). Indeed, IgA-deficient mice and humans show increased susceptibility to gastrointestinal infections and inflammatory diseases, such as celiac disease or inflammatory bowel disease (Harriman et al., 1999; Johansen et al., 1999; Ludvigsson et al., 2016). Gut microbiota drives IgA production, since germ-free mice show a drastic reduction in mucosal IgA-secreting B cells (Moreau et al., 1978). Most intestinal commensals are IgA coated in situ, as shown by combined flow cytometry sorting and 16S ribosomal DNA sequencing (Kawamoto et al., 2012; Palm et al., 2014; Bunker et al., 2015; Kau et al., 2015). IgA predominantly binds colitogenic and commensal bacteria of the small intestine (Palm et al., 2014; Bunker et al., 2015). Mouse microbiota-reactive IgA antibodies were shown to target a broad pattern of commensals at the clonal level (Okai et al., 2016; Bunker et al., 2017).

Recent observations in mice highlighted a role for several commensals in the induction of serum IgA, binding in return a restricted fraction of gut microbiota and providing protection to polymicrobial sepsis (Wilmore et al., 2018). Humans, unlike mice, express two subclasses of IgA, IgA1 and IgA2. Whereas IgA1 is predominant in serum, IgA2 is mainly secreted in mucosal compartments (Chiba et al., 1987; Pakkanen et al., 2010). The abundance of the two IgA isotypes varies throughout the intestine (Chiba et al., 1987; Pakkanen et al., 2010). Peyer's patches contain more IgA1$^+$ B cells than lamina propria, whereas, in contrast, colon contains mainly B cells that secrete IgA2, a subclass endowed with enhanced resistance to the action of bacterial proteases, as compared with IgA1 (He et al., 2007). In general, IgA2 class switching occurs through a CD4$^+$ T cell–independent pathway, while IgA1 requires the activation of B cells by CD4$^+$ T cells through CD40–CD40 ligand interaction

[1]Sorbonne Université, Institut national de la santé et de la recherche médicale, Centre d'Immunologie et des Maladies Infectieuses, Assistance Publique Hôpitaux de Paris, Hôpital Pitié-Salpêtrière, Paris, France; [2]Institute of Pharmacology, University of Bern, Bern, Switzerland; [3]Université Paris Diderot Paris 7, Department of Clinical Immunology, Hôpital Saint-Louis, Assistance Publique Hôpitaux de Paris, EA 3518, Paris, France; [4] Micalis Institute, INRA, AgroParisTech, Université Paris-Saclay, 78350, Jouy-en-Josas, France; [5]Unit of Antibodies in Therapy and Pathology, Institut Pasteur, UMR1222 Institut national de la santé et de la recherche médicale, Paris, France; [6]EA 4043, Unité Bactéries Pathogènes et Santé, Université Paris-Sud, Université Paris-Saclay, Châtenay-Malabry, France; [7]Division of B Cell Immunology, German Cancer Research Center, Heidelberg, Germany; [8]Sorbonne Université, Assistance Publique Hôpitaux de Paris, Hôpital Pitié-Salpêtrière, Paris, France; [9]Department of Surgery, Beth Israel Deaconess Medical Center, Harvard Medical School, Boston, MA.

*D. Sterlin, J. Fadlallah, and O. Adams contributed equally to this work; Correspondence to G. Gorochov: guy.gorochov@sorbonne-universite.fr; D. Sterlin's present address is Unit of Antibodies in Therapy and Pathology, Department of Immunology, Institut Pasteur, Paris, France.

and the secretion of TGF-β (He et al., 2007; Coffman et al., 1989). It is widely accepted that microbial capsular polysaccharides and lipopolysaccharides are major targets of commensal-specific antibodies derived from T cell–independent pathways (Bunker et al., 2015; Stowell et al., 2014). It could thus be speculated that the IgA2 repertoire might contain a broader spectrum of microbial carbohydrate–specific antibodies. Overall, the extent to which each of these two subclasses interacts with intestinal commensals along the intestine remains enigmatic.

We compared polyclonal reactivity of secretory IgA1 and IgA2 toward ileum and colon human microbiota and further investigated the specificity of IgA2 at the clonal level. Our results argue that human IgA antibodies are both promiscuous and selective in their interaction with the microbiota.

Results

Broad but differential glycan recognition by serum IgA1 and IgA2

To decipher the repertoire of carbohydrate-specific IgA, we used glycan microarray technology. Comparison of the glycan recognition profiles of pooled human IgA1 and IgA2 revealed a broad recognition pattern of carbohydrate structures by both classes of antibodies, although only 15 glycans were cotargeted by both IgA1 and IgA2 (Fig. 1, A and B).

The terminal carbohydrate moiety has been shown to be a critical determinant of glycan-specific antibody responses (Schneider et al., 2015), which could explain the lack of overlap of IgA1 and IgA2 carbohydrate repertoires. Glycan microarray screening of pooled human serum–derived IgG revealed prominent recognition of galactose-α (Galα)–terminated glycans, which include major xenoantigens (Griesemer et al., 2014), but limited binding to sialoglycans containing human N-Acteylmeuraminic acid (Neu5Ac) or nonhuman N-Glycolylneuraminic acid (Neu5Gc; Schneider et al., 2015). Strikingly, Galα-terminated glycans were almost exclusively recognized by IgA2 (Fig. 1 C). Preferential recognition by IgA2 was observed for both Neu5Ac- and Neu5Gc-terminated sialoglycans, while N-Acetylglucosamine (GlcNAc)–terminal glycans were equally bound by IgA1 and IgA2. By consulting the Bacterial Carbohydrate Structure Database, we determined that among the 610 glycans on the microarray, 137 structures were identified as bacterial antigens, including 16 Galα-terminated structures. We observed that bacterial antigens, excluding Galα-terminated structures (n = 121), had a similar recognition profile when compared with the entire glycan microarray dataset (Fig. 1 D). Thus, the overall structure of the glycans has an impact on the induced IgA1 and/or IgA2 immunogenicity. These results also demonstrate that IgA2 widely recognizes bacterial antigens and that this phenomenon is more evident for Galα-structures.

Finally, we noticed that 3 out of the 10 host glycans displayed on the microarray, known to serve as attachment sites for bacteria in various mucosal compartments (Schneider et al., 2015), were preferentially bound by IgA2, as compared with IgA1 (Fig. 1 E). The latter findings support the conclusion that IgA tempers bacterial activity, not only through direct interaction with their surface antigens but also by interfering with their host ligands. More host attachment sites should be tested in order to determine whether IgA2 is preferentially involved in recognizing host glycans used for bacterial adhesion.

The secretory component modestly contributes to glycan binding

The above study was conducted with serum IgA. However, in gut lumen, dimeric IgA is associated with the secretory component that mediates binding to Gram-positive bacteria irrespective of antibody specificity. Using glycan array technology, we assessed secretory component binding to carbohydrates and found 27 glycans that were specifically recognized by the secretory component (Fig. S1 A). These results point out that, in vivo, the secretory component may further enlarge the spectrum of IgA binding to microbiota; however, the glycan-binding pattern remains much wider for IgA alone than for the secretory component.

Gut bacteria are predominantly targeted by IgA2

We observed partial overlap of microbial carbohydrate reactivity between serum IgA1 and IgA2, while IgA2 was found to exhibit a broader spectrum of microbial specificities. We attempted to test whether the carbohydrate reactivity patterns observed with IgA1 and IgA2 reflected microbial recognition in vivo using bacterial flow cytometry analysis (Moor et al., 2016). Because gut contains not only the highest concentration of microbial antigens but also both subclasses of IgA, we investigated the extent of secretory IgA binding to gut commensals. We used isotype-specific secondary antibodies to probe naturally IgA-coated microbiota of healthy donors. We first ruled out cross-reactivity of anti-IgA1 and anti-IgA2 antibodies by probing human B cells that are known to express only one antibody isotype and determined that virtually no double-positive cells were present when B cells were incubated with fluorescent anti-IgA1 and anti-IgA2 antibodies (Fig. S1 B). Using these reagents, we observed that IgA2 accounted for most commensal binding in fecal microbiota of healthy donors (Fig. 2 A, upper panel).

Convergent IgA1 and IgA2 responses

While IgA1 bound the same commensal bacteria as IgA2, other commensals were targeted by the latter isotype only (Fig. 2 A). Whereas the frequency of $IgA2^+IgA1^+$ and $IgA2^+IgA1^-$ fractions varied among individuals (1.95% [0.12–7.27%] vs. 3.19% [0.69–17.99%] of all fecal bacteria; Fig. 2 B), the $IgA2^-IgA1^+$ fraction was always negligible (0.08% [0–1.00%]; Fig. 2 B). Flow cytometry analysis showed that IgA-coated bacteria segregated into two fractions, depending on median fluorescence intensity: IgA^{low} and IgA^{bright} staining. Dual staining by IgA1 and IgA2 was associated with the IgA^{bright} fraction, whereas the IgA^{low} fraction corresponded to $IgA2^+IgA1^-$ bacteria (Fig. S1 C). Because ileal Peyer's patches contained more $IgA1^+$ than $IgA2^+$ B cells (He et al., 2007), we also profiled total IgA and IgA subclass binding in ileal contents. As expected (Bunker et al., 2015), we found higher proportions of IgA-coated microbiota in the ileum than in the fecal compartment (53.6% [44.6–79.4%] vs. 9.15%

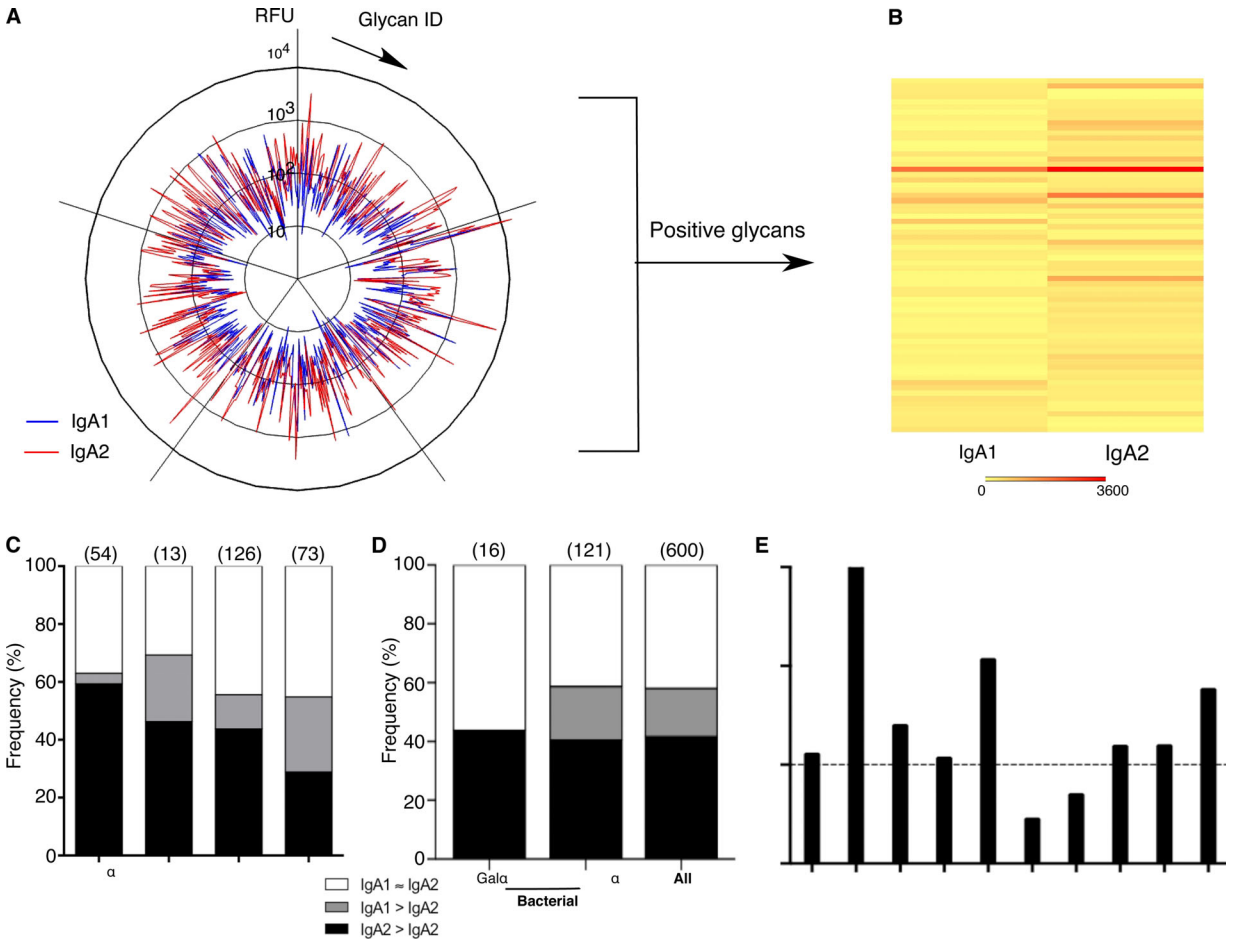

Figure 1. **Carbohydrate-binding profile of polyclonal IgA1 and IgA2 antibodies. (A)** Glycan reactivity of serum polyclonal IgA1 and IgA2 (n = 5 healthy donors pooled in one experiment). Each peak represents an individual glycan recognized by IgA1 (blue line) or IgA2 (red line). **(B)** Heatmap diagram depicting glycans recognized by IgA1 or IgA2. Each row represents an individual glycan. **(C)** Preferential recognition of distinct terminal carbohydrate moieties by serum polyclonal IgA1, IgA2, or both. Terminal carbohydrate moieties equally recognized by both IgA1 and IgA2 are depicted in white. Terminal moieties preferentially recognized by IgA1 or IgA2 are showed in gray or black, respectively. **(D)** Isotype-dependent recognition of Galα-terminal structures of bacterial origin and other bacterial antigens excluding Galα-terminal antigens (without Galα) by serum polyclonal IgA, as compared with entire glycan microarray dataset. Terminal carbohydrate moieties equally recognized by both IgA1 and IgA2 are depicted in white. Terminal moieties preferentially recognized by IgA1 or IgA2 are showed in gray or black, respectively. **(E)** Differential isotype binding to bacterial attachment sites.

[1.61–34.6%]; Fig. S1 D). A large proportion of ileal commensals were bound by both IgA1 and IgA2 (37.4% [19.2–55.2%]; Fig. 2 A, lower panel), indicating that the convergence of IgA1 and IgA2 responses is compartment independent.

Convergent IgM and IgA responses

We observed significant IgM staining (IgM-coated bacteria ≥1%) in the fecal microbiota of only 5 out of 20 healthy donors (0.32% [0.04–7.51%]; Fig. 2 C) in line with observations suggesting that IgM binds mucosal (Magri et al., 2017) rather than luminal (Fadlallah et al., 2018) communities in the colon. Among these five fecal samples and five other ileal samples, we searched for IgM, IgA1, or IgA2 overlapping binding. Like IgA-coated bacteria, IgM-coated bacteria were more abundant in the ileum. Indeed, the frequency of IgM-coated bacteria exceeded 20% in three out of five ileal specimens (24.10% [0.65–74.71%]; Fig. 2 C). We found that IgM-bound bacteria were also largely bound by both IgA1 and IgA2 (Fig. 2, D–F). Hence, IgM converges toward IgA-bound microbes, both in the ileum and in the colon lumen.

IgA2 also predominates in early life

A constant ratio of IgA1 to IgA2 has been reported in serum throughout childhood, which implies that there is no delay in the production of one isotype as compared with the other (Schauer et al., 2003). However, little is known about the establishment of secretory IgA subclasses in early life. Because analysis of IgA-coated bacteria is complicated by the presence of breast milk–derived IgA during the first months of life, we selected fecal samples from eight formula-fed neonates (mean age: 5 mo; age range: [3–5] mo) and quantified their proportions of IgA-, IgA1-, and IgA2-bound microbiota. Like in adults, mostly $IgA2^{+}IgA1^{+}$ and $IgA2^{+}IgA1^{-}$ bacteria were detected, while $IgA2^{-}IgA1^{+}$ cells were rare among neonatal fecal microbiota (3.23% [0.69–6.7%], 3.96% [2.94–32.8%], and 0.08% [0.00–2.08%], respectively; Fig. 2 G), suggesting that both autologous IgA1 and IgA2 are

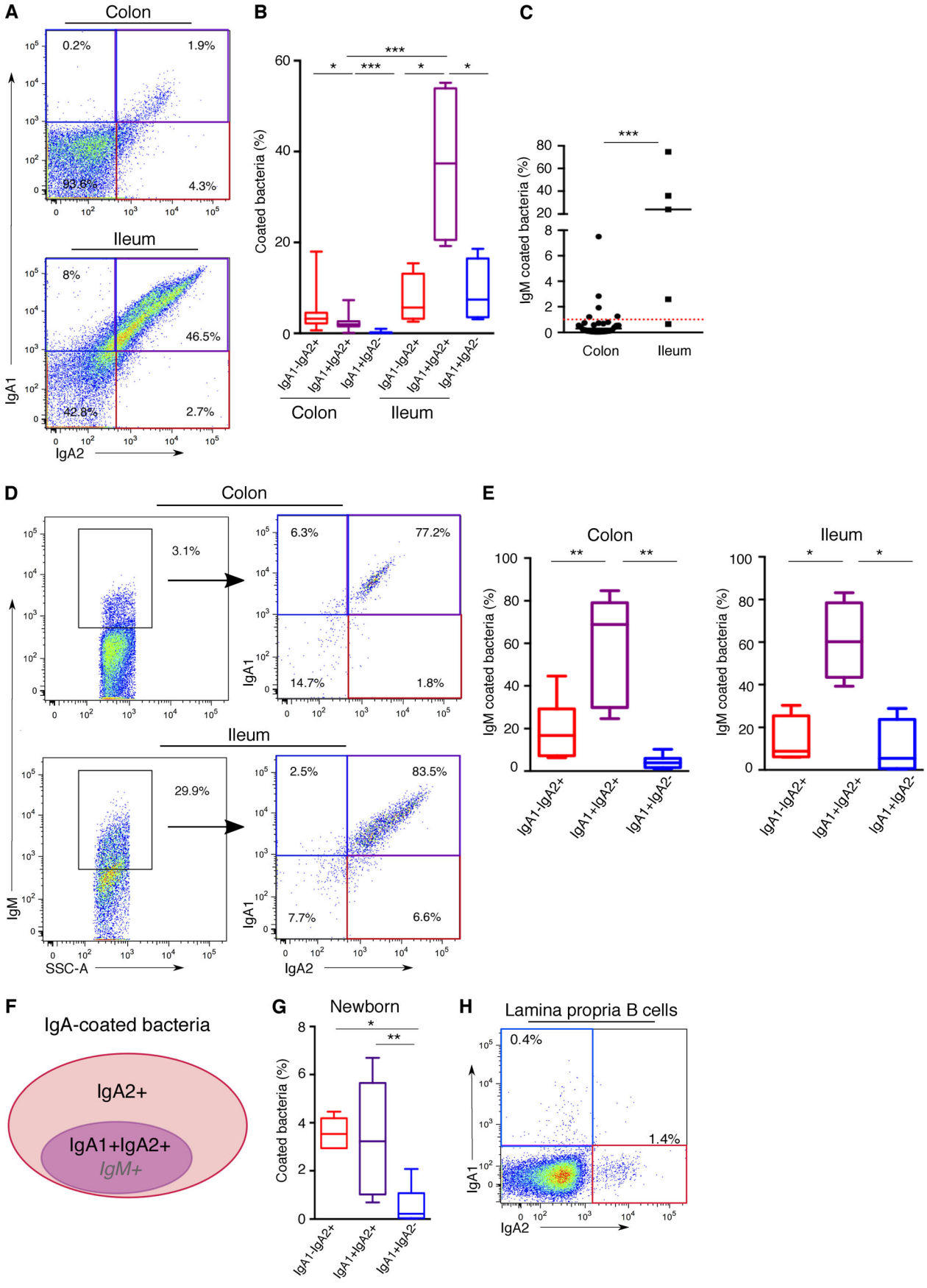

Figure 2. **IgA1 targets IgA2-coated bacteria. (A)** Representative flow cytometry analysis of endogenous IgA1 and IgA2 fecal or ileal microbiota coating. **(B)** Endogenous IgA1 and IgA2 microbiota coating levels in 20 fecal and 5 ileal healthy samples. Data are cumulative from three independent experiments. Error bars represent minimum and maximum values. P values were calculated using the Mann-Whitney test (colon vs. ileum) or Wilcoxon test (*, P < 0.05; ***, P < 0.001). **(C)** Endogenous IgM microbiota coating levels in 20 fecal and 5 ileal healthy samples (two independent experiments). Dark bars indicate medians. Red dotted line represent significant the positive cutoff. P values were calculated using the Mann-Whitney test (***, P < 0.001). **(D)** Left: Representative flow cytometric analysis of endogenous IgM-coated fecal or ileal microbiota. Right: Representative flow cytometric analysis of endogenous IgA1 and IgA2 binding in IgM-coated fecal or ileal microbiota (two independent experiments). SSC-A, side scatter area. **(E)** Endogenous IgM microbiota coating levels in 20 fecal and 5 ileal healthy samples (two independent experiments). Error bars represent minimum and maximum values. P values were calculated using the Mann-Whitney test (**, P < 0.01; *, P < 0.05). **(F)** Model Venn diagram showing overlap among endogenous IgA1, IgA2, and IgM binding in IgA-coated microbiota. **(G)** Endogenous IgA1 and IgA2 microbiota–coating levels in eight fecal samples from formula-fed neonates (two independent experiments). Error bars represent minimum and maximum values. P values were calculated using the Wilcoxon test (*, P < 0.05; **, P < 0.01). **(H)** Flow cytometric analysis of IgA1 and IgA2 expression on colonic lamina propria B cells from a 3-mo-old infant (one experiment).

involved in the coating of the developing microbiota very early on. To corroborate these findings, we took advantage of a single colon tissue specimen obtained from a 3-mo-old infant and verified its IgA1 and IgA2 B cell content. As expected, lamina propria IgA2$^+$ B cells were more abundant that IgA2$^+$ B cells in this sample (1.4% vs. 0.4%; Fig. 2 H). Thus, like in adults, the IgA2 isotype predominates in infants, although IgA1 nevertheless cobinds IgA2-coated bacteria.

Interindividual variability of IgA1- and IgA2-binding profiles

We next analyzed the composition of subclass-bound bacteria in fluorescence-activated cell-sorted IgA1$^+$ and IgA2$^+$ populations and identified bacterial species by 16s ribosomal RNA (rRNA) sequencing. Of note, as all IgA1-coated bacteria were also bound by IgA2, the IgA1-sorted fraction included only IgA2$^+$IgA1$^+$–coated bacteria, whereas the IgA2-sorted fraction both contained IgA2$^+$IgA1$^+$ and IgA2$^+$IgA1$^-$ (referred as IgA2$^+$IgA1$^{+/-}$ in the text), with IgA2$^+$IgA1$^-$ bacteria being predominant (IgA2$^+$IgA1$^-$/IgA2$^+$IgA1$^+$ ratio >2). We first examined the whole microbiota composition and found interindividual variability at phylum and genus levels (Fig. S2, B–D). The microbial diversity, as well as bacterial composition, differed between donors, as shown by the Shannon index (2.98 [2.85–3.30]; Fig. S2 C). With respect to the sorted fractions, within a single donor, IgA1 and IgA2 binding identified distinct patterns of bacteria at the family level. For example, in a given healthy donor, Bifidobacteriaceae were enriched in the IgA2$^+$IgA1$^+$–coated fraction, while Ruminococcaceae were predominant in the IgA2$^+$IgA1$^{+/-}$–enriched fraction, as compared with the whole microbiota of the same donor (Fig. S2 E). We also noticed interindividual variability of IgA1- and IgA2-binding profiles at the family level, suggesting that the preferred targets of IgA1 and IgA2 are dependent on microbiota composition rather than on microbial phylogeny (Figs. 3 A and S2 E).

We next focused on the genus level and determined the breadth of bacteria coated by IgA1 and IgA2 by comparing the relative abundance of bacteria genera in each of the fractions. Genera were present at similar frequencies in both IgA2$^+$IgA1$^+$– and IgA2$^+$IgA1$^{+/-}$–sorted fractions (median of genera relative abundance 0.00048 [0.00018–0.0038] vs. 0.0019 [0.00041–0.00276], respectively, P = 0.81; Fig. 3 B). Moreover, the two fractions did not significantly differ from input microbiota in terms of bacterial diversity (Shannon index 2.36 [1.3–2.88], P = 0.19 vs. 2.31 [1.97–2.86], P = 0.13, respectively; Fig. S2 C), indicating that both IgA subclasses coat highly diverse commensals.

Core IgA1$^+$IgA2$^+$ microbiota among an extended IgA2$^+$ bacterial repertoire

The results thus far indicate that IgA2$^+$IgA1$^+$– and IgA2$^+$IgA1$^{+/-}$–sorted fractions are diverse. Their bacterial composition is not only different between donors (Fig. 3, A and B) but also distinguishes itself from the input fraction within a single donor (Fig. 3 C). Thereafter, we narrowed the analysis down to the 19 most frequent genera that were present in ≥80% of the IgA-coated fractions. To unravel IgA subclass specificities for microbes, we compared IgA2$^+$IgA1$^+$– and IgA2$^+$IgA1$^{+/-}$–sorted fractions by calculating log-based enrichment indexes (EIs; see calculation details in Materials and methods). This calculation allows us to deduce bacteria preferentially targeted by IgA2 alone compared with dually coated bacteria. Eleven genera were preferentially counted in the IgA1$^+$IgA2$^+$ subset, while eight genera tended to be more frequent in the IgA2$^+$IgA1$^{+/-}$–coated bacteria (Fig. 3 D). Interestingly, genera derived from Actinobacteria (*Rhodococcus*, *Bifidobacterium*, and *Arthrobacter*) were all enriched in dually stained bacteria. Instead, genera derived from Bacteroidetes (*Prevotella*, *Flavobacterium*, and *Bacteroides*) were preferentially found in the IgA2$^+$IgA1$^{+/-}$ fraction (Fig. 3 D), particularly *Flavobacterium* (IgA2$^+$IgA1$^{+/-}$ EI 1.69 [0.28–2.23] vs. IgA2$^+$IgA1$^+$ EI −0.11 [−2.63 to 0]; P < 0.05; Fig. 3 E).

We sought to validate these observations by staining microbiota and representative bacterial strains with IgA purified from maternal milk. The latter antibodies are more abundant and might be taken as representative of gut IgA, as in mammary glands, and IgA plasma cells are mainly derived from gut B cells, in agreement with the observation that some breast milk antibodies recognize gut antigens (Lindner et al., 2015). Moreover, flow cytometry analysis is facilitated since breast milk contains equal quantities of both subclasses, in contrast to free fecal IgAs that comprise mainly IgA2 (Ladjeva et al., 1989). We first confirmed that breast milk–IgA antibodies targeted microbiota from an IgA-deficient patient (Fig. S3 A). We then confirmed that both IgA1 and IgA2 bound *Bifidobacterium longum*, while *Bacteroides vulgatus* was only recognized by IgA2 (Fig. 3 F).

Taken together, these results demonstrate that both IgA subclasses bind a diverse spectrum of commensals. In the small intestine, IgA1 targets the same commensal bacteria as IgA2 in a balanced manner, while in the colon, IgA2 preferentially targets several genera (typically derived from Bacteroidetes).

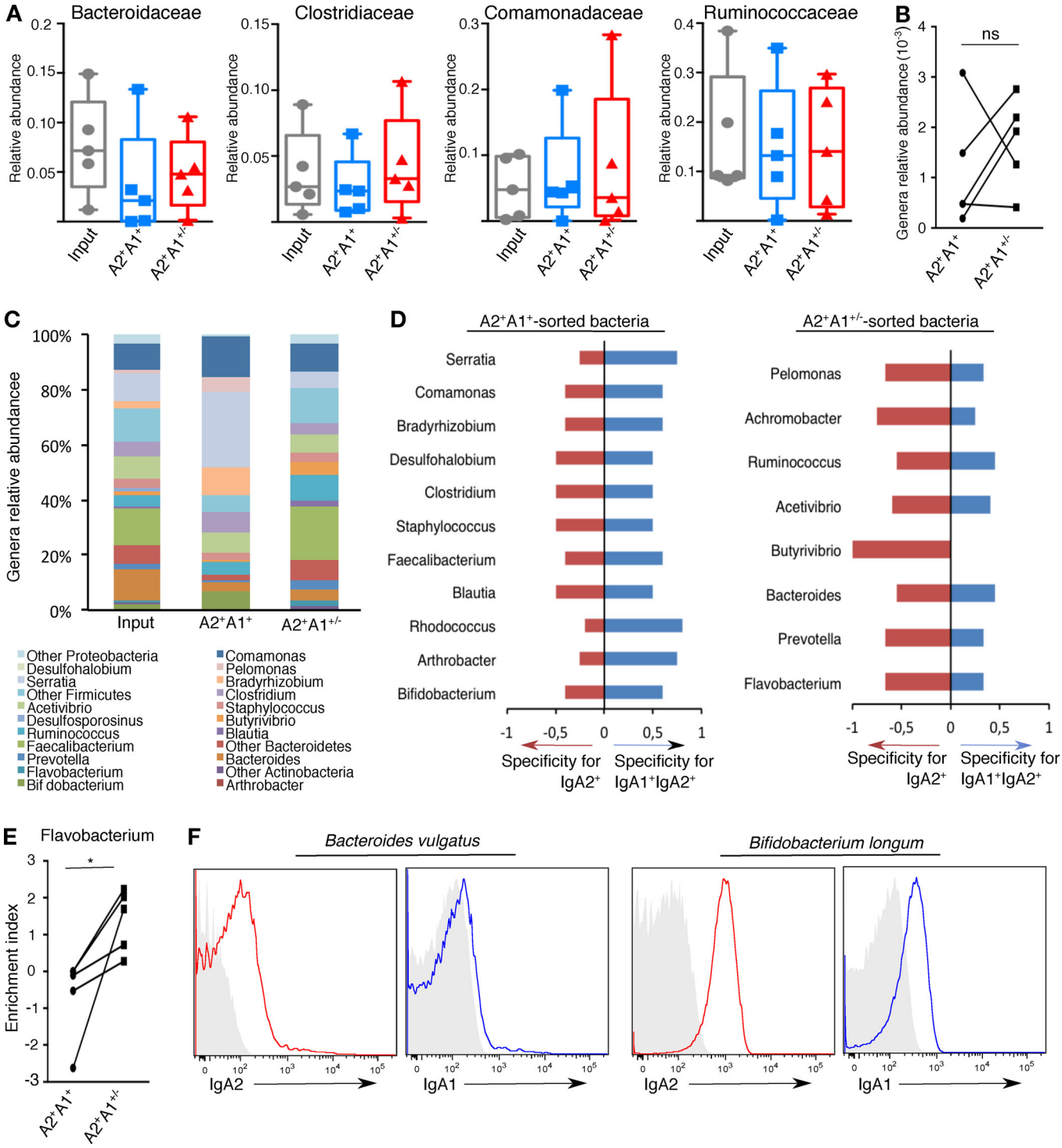

Figure 3. **IgA1 coordinates with IgA2 to coat distinct commensal bacteria. (A)** Median relative abundance of the four most frequent families in sorted fractions from five healthy donors. Each dot represents one donor. Boxes extend from the 25th to the 75th percentiles. Error bars represent minimum and maximum values. **(B)** Median relative abundance of genera from IgA1$^+$IgA2$^+$ and IgA2$^+$ fractions from five healthy donors. Each dot represents one donor. **(C)** Relative abundance of indicated top 19 most abundant genera in sorted fractions from one healthy donor. **(D)** Specificity of IgA subclass targeting for all individuals analyzed (n = 5). Number of samples in which a given genera had a positive indicated IgA subclass EI, divided by the total number of samples. The formula is detailed in Materials and methods. **(E)** *Flavobacterium* enrichment in IgA2$^+$ as compared with IgA1$^+$IgA2$^+$ fractions. Each dot represents one donor. P values were defined using the Wilcoxon test (*, P < 0.05). **(F)** Binding of purified breast milk IgA to indicated bacterial strains. Monoclonal IgA isotype control (gray-filled histogram) was included as negative flow cytometry control. The same experiment was repeated twice. ns, not significant.

Both IgA1 and IgA2 induce cytokine production

Because IgA1 simultaneously binds IgA2-coated bacteria, we investigated whether IgA1 and IgA2 differ in their function. Several compelling arguments support a role of IgA through FcαRI expressed on monocytes and macrophages in mucosal immunity (Aleyd et al., 2015; Hellwig et al., 2001; Balu et al., 2011). We therefore determined how IgA subclass opsonization affected the production of cytokines by macrophages. We selected *Staphylococcus haemolyticus* as a common commensal recognized by both IgA1 and IgA2 (Fig. 3 D) and incubated free or IgA-opsonized bacteria with monocyte-derived macrophages. In accordance with previous reports (Hansen et al., 2017), we observed that IgA opsonization strongly enhanced cytokine production by these cells (Fig. S3 B). Both IgA1 and IgA2 increased the production of IL-6 and TNF-α, yet IgA1 tended to induce more IL-10 than IgA2.

Human gut lamina propria–derived monoclonal IgA

Colonic bacteria are thus predominantly bound by the IgA2 isotype. To address the issue of IgA2 specificity for human gut microbiota at a single-cell level, we generated fully human IgA mAbs derived from the colonic lamina propria of three healthy donors. We transduced highly purified intestinal IgA$^+$ memory B cells with a Bcl-6/Bcl-xL–expressing retrovirus (Kwakkenbos et al., 2010), resulting in the establishment, under limiting dilution conditions, of long-term clonal B cell cultures (Fig. S4 A). Each B cell line was self-renewing and showed a stable expression of IgA and the activation markers CD38 and CD95 for the duration of the study (Fig. S4 B). Eight monoclonal IgA antibodies of unrelated sequences (Table S1) were detected as dimeric IgA in culture supernatants (Fig. S4 C). Previously characterized monomeric human IgA2 clones directly obtained by single-cell PCR amplification of the variable Ig genes of isolated colonic cells (Benckert et al., 2011) were also tested.

Discrete bacterial populations are brightly stained by gut-derived IgA antibodies

To characterize the commensal reactivity of these IgA mAbs in the absence of competing interference by naturally occurring IgA, we selected an IgA-deficient microbiota (coined "A") in order to probe antibody–bacteria interactions. It has previously been shown that microbiota complexity is maintained in IgA-deficient patients, without massive perturbations of gut luminal microbes (Fadlallah et al., 2018). All eight IgA mAbs bound restricted microbiota fractions (Fig. 4, A and B). However, both staining intensity (range of median fluorescence intensity, 2,080–10,724) and frequency of bound bacteria (0.79–1.66% of mAb-coated bacteria) differed between mAbs. Neither the frequency of mAb-coated bacteria nor that of somatic mutations was correlated with the staining intensity (Fig. 4 C).

IgA binding to microbiota is mostly Fab mediated

To test whether gut-derived IgA mAbs interacted in a Fab or Fc-dependent manner, we first tested an irrelevant human anti-TNP IgA. The latter did not bind to microbiota, suggesting that gut-derived antibody binding might be mostly Fab mediated (Fig. 4 A). However, we speculated that the anti-TNP IgA used could possibly bear a different glycosylation pattern compared with gut-derived IgA that may account for its lack of microbiota interaction. We therefore also investigated gut IgA2 mAbs bearing IgG1 constant domains (Benckert et al., 2011). Before measuring their reactivity to microbiota, we first ruled out the presence of IgG-bound bacteria in another IgA-deficient microbiota (microbiota B), in agreement with the lack of IgG transport to the intestinal lumen (Fig. S4 D). Although their microbiota avidity might be lower as compared with parental dimeric IgA, all but one IgA2 Fab/IgG1 Fc monomeric chimeras bound fecal microbiota (0–1.13% of mAb-coated bacteria; Fig. 4, D and E). In line with results obtained with dimeric IgA mAbs (Fig. 4 C), the frequency of monomeric mAb-coated bacteria was not correlated with staining intensity (Fig. 4 F). Together, these results demonstrate that the IgA mAbs tested bind microbiota in a Fab-dependent manner.

Intestinal IgA clones target highly diverse commensal bacteria

To identify commensal bacteria bound by individual monoclonal IgA, we characterized mAb-bound (mAb$^+$) sorted fractions by 16S rRNA gene sequencing (Fig. 4 G). All mAbs tested recognized the four major phyla, namely Actinobacteria, Bacteroidetes, Firmicutes, and Proteobacteria, but each one exhibited a unique binding profile (Fig. 4 H). Genus-level analysis corroborated these distinct binding patterns and highlighted IgA cross-reactivity with numerous genera, irrespective of their microbial phylogeny (Fig. 4, I and J). Both series of mAbs, generated either with IgA2 or IgG1 Fc domain, bound various genera (Fig. 4, I and J). These data therefore indicate that a single IgA might recognize a wide panel of bacteria. Because mAb reactivity extended to unrelated genera, we tested whether genus abundance might influence mAb-binding patterns. We found that genera in mAb$^+$ and mAb$^-$ fractions did not differ in terms of relative abundance (median of genera relative abundance 0.00123 [0.000284–0.0056] in the mAb$^+$ fraction vs. 0.0008 [0.00026–0.00159] in the mAb$^-$ fraction, P = 0.27; Fig. 4 K). Moreover, 12 out of the 50 most abundant genera (*Eggerthella*, *Bacteroides*, *Parabacteroides*, *Anaerostipes*, *Kingella*, *Neisseria*, and *Pelomonas* in microbiota A and *Tissierella*, *Peptostreptococcus*, *Paenibacillus*, *Microbacteriuma*, and *Helcococcus* in microbiota B) were not targeted by the tested mAbs (Fig. S4, E and F), thereby implying that IgA antibodies react with various commensal microbes regardless of their bacterial richness. As expected, mAb-binding profiles included *Ruminococcus*, *Roseburia*, *Clostridium*, and *Blautia* previously described as common IgA targets in humans (Fig. 4, I and J; D'Auria et al., 2013; Palm et al., 2014; Magri et al., 2017).

IgA clones exhibit private microbiota-binding patterns

The mAb-binding patterns were characterized in a quantitative manner by calculating a log-based EI at the genus level, followed by the application of a hierarchical clustering algorithm (Fig. S4, E and F). All mAbs were highly cross-reactive against a median of 19 genera among the 50 most abundant (range, 8 to 27; Fig. S4, E and F). Neither the frequency of somatic mutations nor the staining intensity correlated with the number of target genera, according to positive EIs. In addition, EIs varied among the target

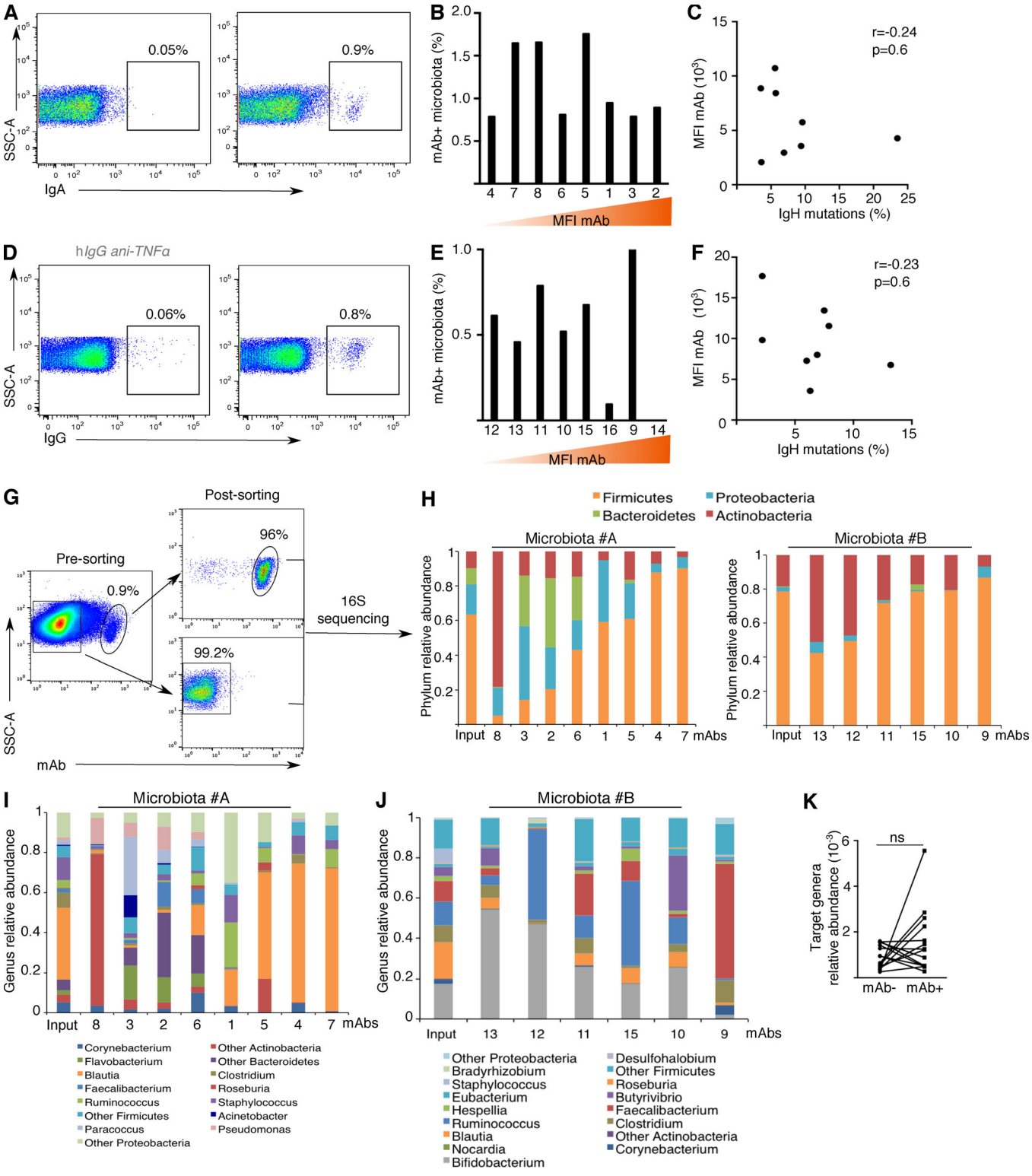

Figure 4. **Human monoclonal IgA target highly diverse commensal bacteria. (A)** Representative flow cytometry plot of microbiota reactivity for mAb#2 and human IgA2 anti-TNP. mAbs 1–8 are gut monoclonal IgA2 expressed as dimeric IgA. SSC-A, side scatter area. **(B)** mAb coating of IgA-free microbiota. mAbs are classified in increasing fluorescence intensity order (median fluorescence intensity [MFI], range 2,080–10,724). The same experiment was repeated twice. **(C)** Somatic mutations of mAbs are not correlated to IgA staining intensity. Somatic mutations in the V-region of *IGH* gene were analyzed. Nonparametric Spearman correlation was calculated. **(D)** Representative flow cytometry plot of microbiota reactivity for mAb 10 and human IgG1 anti-TNFα. mAbs 9–16 are gut monoclonal IgA2 expressed as IgG1 (Benckert et al., 2011). **(E)** mAb coating of IgA and IgG-free microbiota. MAbs are classified in increasing fluorescence intensity order (MFI, range 3,585–17,683). The same experiment was repeated twice. **(F)** Somatic mutations of mAbs are not correlated to mAb staining intensity. Somatic mutations in V-region of *IGH* gene were analyzed. Nonparametric Spearman correlation was calculated. **(G)** mAb⁺ and mAb⁻ fractions of IgA-free gut microbiota were sorted by flow cytometry, and their composition was analyzed by 16S rRNA sequencing. **(H)** Relative abundance of phyla in whole

microbiota (input) and mAb+ fractions. Microbiota A is IgA-free, while microbiota B is IgA- and IgG-free. 16S rRNA sequencing data were from two independent experiments. **(I)** Relative abundance of genera in whole microbiota A (input) and mAb+ fractions. **(J)** Relative abundance of genera in whole microbiota B (input) and mAb+ fractions. **(K)** Scatter dot plot of median relative abundance of genera from mAb+ and mAb− fractions. ns, not significant.

genera of the mAbs, indicating that they might bind variant genera with different affinities. Higher EIs could also be accounted for, in case a mAb recognized more species within a genus.

To confirm the validity of the mAb targets identified by 16S rRNA sequencing, we also compared mAb IgA binding to representative bacterial strains isolated from human fecal samples. We previously calculated that only mAbs 1, 2, 3, 9, and 10 were associated with positive *Staphylococcus* EIs, while mAbs 4 and 7 were not. Accordingly, the latter two clones did not bind *Staphylococcus aureus* or *S. haemolyticus* (Fig. S4 G). Interestingly, while mAbs 1, 2, and 3 indeed bound both bacteria, mAbs 9 and 10 only bound *S. haemolyticus*, supporting the conclusion that some IgAs, such as mAbs 9 and 10, target only distinct species within a genus.

In summary, we conclude that IgA clones recognize a broad spectrum of commensal species regardless of their phylogeny, while each of the mAbs generated in the present study exhibited a private binding profile.

Private glycan cross-reactive patterns of IgA clones

We hypothesized that shared structures between numerous bacterial species could contribute to the observed IgA cross-reactivity. Commensal bacteria express a wide diversity of glycans, and it is frequently assumed that bacterial surface carbohydrates are among the common targets of intestinal IgA (Bunker et al., 2017). Moreover, glycosylation is a very common posttranslational modification that might create shared epitopes between various bacterial species, independently of their phylogeny (Grangeasse et al., 2015; Macek et al., 2008; Bastos et al., 2017). We therefore extended our analysis by screening human IgA mAbs on a glycan microarray displaying 660 different synthetic carbohydrate structures. Fig. 5 A illustrates the binding profile for mAb 1 expressed as mean relative fluorescence units (RFUs). For 17 glycans, for which binding was above background, the antibody-binding ratio (ABR) of human IgA mAbs was calculated relative to an isotype-matched control mAbs, followed by hierarchical clustering analysis (Schneider et al., 2015). Five glycan structures were specifically recognized by the mAbs tested (Fig. 5, B and C). It is noteworthy to mention that three out of the five structures are epitopes of known bacterial origin (Sugahara et al., 1979; Arbatsky et al., 2000; Bystrova et al., 2000; Tsepilov and Beloded, 2015). Only two glycans, 804 (Galβ1-1GlcNAcβ-OCH2CH2)2 and 630 (GlcAβ1-3GlcNAcβ1-4)20, were bound by all mAbs, albeit with different intensities. These results do not imply that IgA2 would only bind glycan antigens, but interestingly, all mAbs tested were glycan cross-reactive. Concurrently, each IgA2 clone tested exhibited a unique glycan-binding pattern.

Bacterial glycans contribute to the IgA–microbiota interaction

The observations described above confirmed that IgA exhibits bacterial and glycan cross-reactivity but do not infer that IgA binding to microbiota is mainly due to glycan recognition. To evaluate whether glycans indeed play a role at the IgA–microbiota interface, we sought to compare IgA binding to microbiota before and after deglycosylation. As shown in Fig. 5 D, enzymatic procedure removal of glycans on gut bacteria resulted in a marked drop in the interaction with monoclonal IgA (median % of decrease and range: 23 [15–28]), indicating a contribution of carbohydrates in the binding. Since much remains to be uncovered concerning glycosylation in prokaryotes, we assumed that the panel of enzymes we used on whole microbiota likely lead to only partial deglycosylation of the latter and a possible underestimation of glycan involvement with IgA binding. We therefore further explored the role of glycans in IgA binding at the bacterial strain level. Since mAbs 9 and 10 recognized *S. aureus*, but not *S. haemolyticus* (Fig. 5 E), we purified their surface glycans and found that both mAbs bound purified peptidoglycan (PG), but not teichoic acid (TA) from *S. aureus*. As expected, no binding to *S. haemolyticus* PG was observed. Together, these observations confirm that glycans do play a role in IgA binding to microbiota.

Cross-reactive IgA bear features of antigen-driven affinity maturation

The above observations all support the view that IgA binds diverse bacterial species. This cross-reactive pattern raised the question of IgA affinity maturation. Cross-reactive antibodies are thought to derive from T cell–independent responses, which generate low-affinity antibodies, referred to as "innate" antibodies, as compared with "classical" antibodies that are thought to originate from T cell–dependent responses, exhibiting both elevated numbers of somatic mutations and high affinity (Pabst, 2012). We observed high numbers of somatic mutations in the Ig gene encoding the variable heavy (VH) chain domain of the IgA clones tested. As shown, higher ratios of nonsilent to silent mutations in the complementary-determining regions (CDRs) 1 and 2 (median 5.5 [0–29.5]) than in the framework regions (FWRs) 1–3 (median 2.3 [0.3–15]; Fig. S5 A) are consistent with an antigen-mediated selection process. Thus, in the gut, the affinity maturation process gives rise to cross-reactive IgA.

A fraction of gut-derived IgA is self-specific

Self-reactive IgA+ plasmablasts account for ≤15% of the normal intestinal plasmablast population (Benckert et al., 2011). To determine whether the microbiota-reactive mAb tested here might also react with self-antigens, we performed indirect immunofluorescence assays with the human epithelial cell line HEp-2000. We first established, as a positive control, that free fecal IgA reacted with nuclear antigens expressed by HEp-2000 cells (Fig. S5 B), thereby confirming that under homeostatic conditions, some intestinal B cells do secrete antibodies with specificity for self-antigens. However, among the 16 mAbs tested, only one showed a nuclear staining pattern (Fig. S5 B).

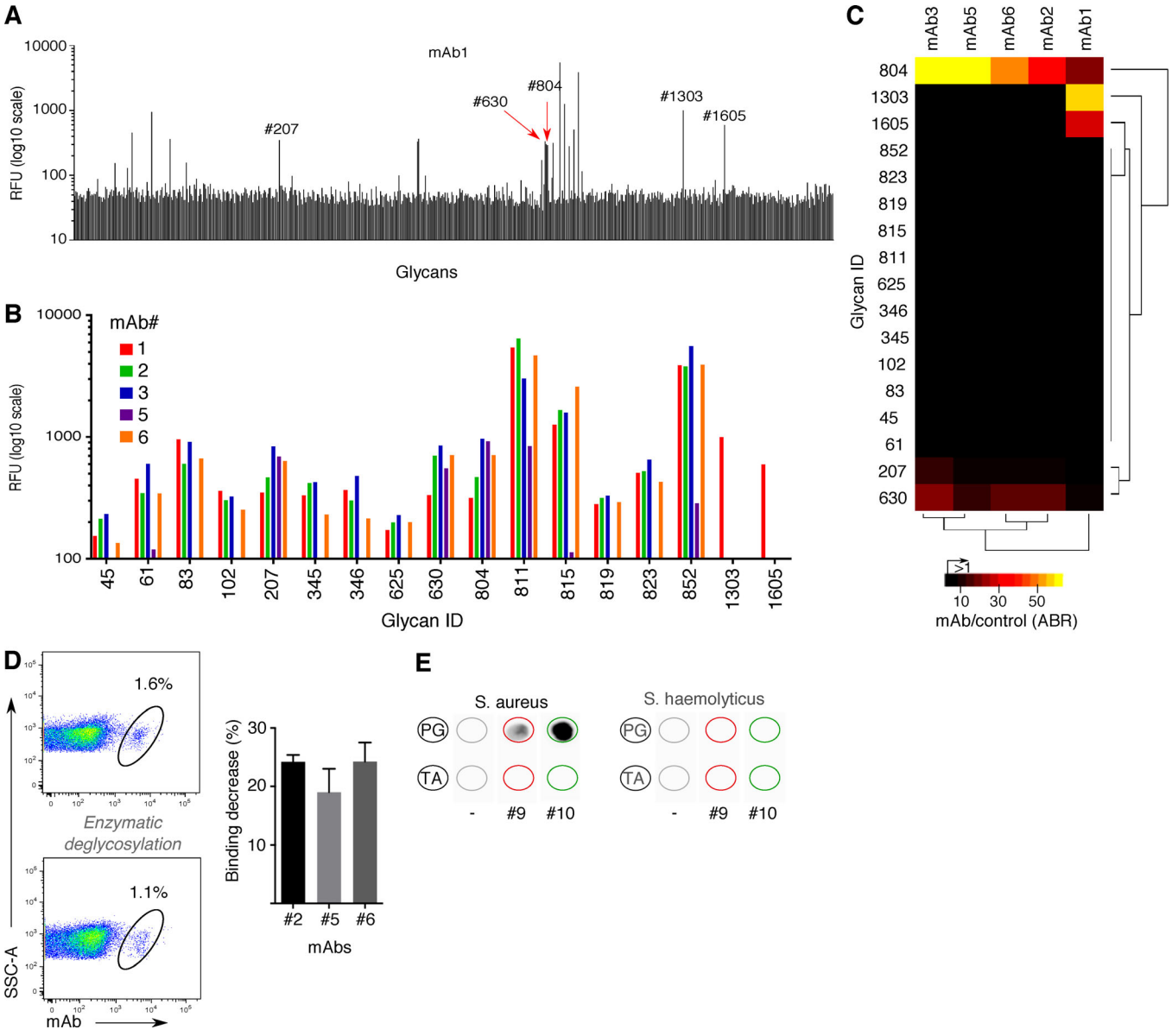

Figure 5. **Microbial surface glycans are common targets of gut human IgA. (A)** Glycan reactivity for five mAbs (5 µg/ml) was assessed using glycan microarray technology (660 structures). Representative median RFUs of mAb1 are shown. Glycan ID numbers of top-bound glycans are indicated. **(B)** The median RFUs for top-bound glycans (above background) are shown for all five mAbs tested. **(C)** The ABR of glycans showing positive reactivity (above background, as in I) was calculated using an isotype control and visualized in an ordered (by dendrogram algorithm) reactivity matrix (heatmap). Each column represents a glycan. Color key is shown. **(D)** Representative flow cytometric dot plot of microbiota-reactivity for mAb 6 after whole-microbiota enzymatic deglycosylation (left). Decrease of mAb binding to microbiota after enzymatic deglycosylation (right). Columns and error bars represent median and maximum values, respectively. The same experiment was repeated twice. SSC-A, side scatter area. **(E)** Representative dot blots of purified PG and lipoteichoic acid (TA) from *S. aureus* and *S. haemolyticus* probed with irrelevant IgG1 (anti-TNFα IgG1), mAb 9, and mAb 10 (gray, red, and green circles, respectively). mAbs 9 and 10 were generated with IgG1 Fc domain. The same experiment was repeated twice.

Collectively, these results suggest that intestinal IgA favors microbiota reactivity over self-antigens.

Discussion

In the present study, we show that human intestinal IgA binds, at the clonal level, a wide subset of microbiota, including commensals from the four most frequent phyla. This reactivity extended to numerous genera, regardless of their phylogenetic distance or their relative abundance. 1 out of 16 mAbs that were generated from intestinal B cells displayed both microbiota-reactivity and self-reactivity, resembling the proportion of 15% self-reactive plasmablasts described in the lamina propria (Benckert et al., 2011). While the molecular basis for this broad antibody reactivity spectrum remains unclear, it has been proposed that IgA binding may involve different affinity interactions with variant antigens of commensal species (Pabst, 2012). Although we could not reliably measure the affinity of antibodies to

bacterial cells, we observed (1) a wide scale of staining intensity and (2) variations across EIs in mAb$^+$ fractions that strongly support low- to high-affinity interactions with commensals. Of note, IgA cross-reactivity does not imply random interactions; on the contrary, IgA interactions appeared rather selective, since, for instance, *S. haemolyticus* evaded some, but not all, IgA antibodies that target *S. aureus*.

Recent studies report the identification of highly abundant clonotypes in peripheral memory, as well as lamina propria, B cells that are cross-reactive (Lee et al., 2016; Rollenske et al., 2018). Quite remarkably, these antibodies are extensively mutated. Here, we found somatic mutation rates comparable to those of IgA$^+$ memory B cells (Berkowska et al., 2011, 2015). Furthermore, replacement/silent ratios point to an antigen-mediated selection, indicating that intestinal cross-specific IgA are likely to originate from an affinity-maturation process. We therefore hypothesize that somatic mutations contribute to the breadth of commensals bound by intestinal IgA, even though reverted murine mAbs were reported to remain poly- and microbiota reactive (Bunker et al., 2017). Consistent with this hypothesis, germline counterparts of human cross-reactive antibodies against *Klebsiella pneumoniae* reportedly lose their binding signature (Rollenske et al., 2018).

It has been previously shown that mouse IgA antibodies react with carbohydrate epitopes (Peterson et al., 2007; Bunker et al., 2017). Our glycan microarray screening data corroborate and extend these observations to humans and further reveal that IgA (in particular IgA2) antibodies recognize a broad range of glycans. Although glycan microarray technology allows for a large number of carbohydrate moieties to be simultaneously assessed, it is still representative of a relatively narrow subset of naturally occurring glycans. In this light, it is remarkable that we observed specific positivity for all human IgA mAbs tested, and the observed glycan cross-reactivity is of considerable significance as well. Indeed, glycosylation is a key posttranslational protein modification that has the capability to modulate protein interactions, and the comprehension of this process might provide insight into evolutionary conservation. Studies relating to bacterial protein posttranslational modifications have identified striking similarities across species, despite their phylogenetic distance (Macek et al., 2008; Grangeasse et al., 2015), reminiscent of our finding that IgA-derived mAbs bind bacteria across genera. While phylogenetically closer species present more overlapping posttranslational modifications, environmental cues modulate them among bacteria (Macek et al., 2008; Grangeasse et al., 2015; Bastos et al., 2017). It seems likely that intestinal conditions influence alterations in protein posttranslational modifications with effects on bacterial fitness and bacterial immunogenicity (Ribet and Cossart, 2010; Butler et al., 2015). Likewise, the gut environment might favor posttranslational pathways that enhance IgA–microbiota interactions.

Our observations raise the issue of the respective functional roles of IgA1 and IgA2 and the respective impact they may have on microbiota diversification along the gastrointestinal tract. We show that both IgA1 and IgA2 induce the production of proinflammatory cytokines, while the regulatory cytokine IL-10 was preferentially induced by IgA1-coated bacteria in vitro (Fig. S3). While IgA2$^+$IgA1$^+$ bacteria are predominant in the ileum, we observe that IgA2 accounts for most colonic commensal binding. Three genera belonging to the phylum Bacteroidetes (*Bacteroides*, *Prevotella*, and *Flavobacterium*) are preferentially recognized by IgA2 in the stool samples. One tentative explanation for this finding might be the longer transit time and the availability of complex polysaccharides in the colon that facilitate the growth of anaerobes such as Bacteroidaceae and Prevotellaceae (Donaldson et al., 2016). In contrast, bacteria coated by both IgA1 and IgA2, such as *Clostridium* species, and additional genera from Actinobacteria (e.g., *Bifidobacterium*) and Proteobacteria phyla (e.g., *Serratia*), are rather small intestine residents (Sekirov et al., 2010; Donaldson et al., 2016). These observations suggest that both IgA1 and IgA2 responses are elicited in the small intestine, while the colon would be the dedicated site for IgA2 responses. Bacteria coated by both subclasses in the colon may represent bacteria originating from the ileum. Indeed, while IgA1$^+$ and IgA2$^+$ B cells are found in similar proportions in the small intestine, IgA2$^+$ B cells are preponderant in the colon (He et al., 2007). One could therefore speculate that IgA2 is essential for diversification of the colonic microbiota, whereas IgA1 is preferentially induced in the ileum.

IgA1 and IgA2 identified distinct patterns of bacteria within a single donor (Fig. 3 C), yet the five healthy donors analyzed in this study only share isotypic-binding trends (Fig. 3 D). The sorting strategy we adopted (i.e., comparing IgA1- and IgA2-sorted cells) introduced crude data noise, as IgA2-sorted cells are necessarily a mixture of IgA2$^+$IgA1$^+$ and IgA2$^+$IgA1$^-$ bacteria. Although the calculation of an EI allows us to deduce isotypic trends, not all subclass targets might have been described in this setting. The high interindividual variability in microbiota composition might also have precluded the identification of more common IgA1 vs. IgA2 targets. However, whereas this indirect sorting approach may, to a certain extent, dilute the signal, it does not invalidate any of the positive results that have been detected. Future work combining more precise sorting (i.e., IgA2$^+$IgA1$^+$ vs. IgA2$^+$IgA1$^-$ pure populations) in a larger healthy donor cohort might therefore identify more bacteria with differential isotype targeting.

Homeostatic secretory IgM responses have been described in humans, but not in mice. Secretory IgM targets a fraction of mucus-embedded commensals that are also coated by IgA in the human colon and ileum (Magri et al., 2017). These observations notwithstanding, we could detect fecal IgM-bound bacteria in luminal content of only 5 out of 20 healthy donors, underscoring the presence of an IgM-bound bacterial gradient from the epithelium to the lumen. IgM may help IgA to localize bacteria to be targeted in a favorable habitat in mucus. Indeed, IgM-bound bacteria are also recognized by IgA1 and IgA2. Consistent with this finding, Magri et al. noticed that IgM coats IgA^{bright} bacteria (Magri et al., 2017).

The mAbs tested for glycan reactivity were all of the IgA2 isotype. In an effort to better understand the molecular basis of the overlapping specificities of IgA1 and IgA2, we performed a comprehensive investigation of the IgA anticarbohydrate repertoire and highlighted a specialization for IgA2 in carbohydrate responses. Our analysis reveals a nonrandom association of

glycan structural features with immunogenicity, especially directed against the monosaccharide moiety at the terminal position. High immunogenicity observed for glycans with terminal Galα is interesting, because this may reflect an important role for IgA2 in response to the microbiota. The finding that both Neu5Ac, a self-antigen, and Neu5Gc, a xenoantigen, showed similar binding profiles for IgA could possibly be explained by the structural similarity of the two sugars. It also supports the notion that terminal carbohydrate moieties influence the balance between immune response and tolerance, IgA being considered more tolerogenic than proinflammatory (Pasquier et al., 2005; Rossato et al., 2015). These results obtained by comparing serum IgA1 and IgA2 remain to be confirmed at the gut secretory IgA level.

In summary, we show that although IgA induction is antigen dependent with highly mutated memory clonotypes, IgA microbiota-binding patterns are broad but nevertheless clonotype specific. Similarly, at the polyclonal level, IgA2 and IgA1 targets are broad and partially overlapping, particularly in the ileum, where $IgA2^+IgA1^+$ bacteria are prevalent among IgA-bound microbiota. In all cases, glycan reactivity accounted not only for the observed cross-reactivity but also for selectivity. IgA2 and IgA1 anticommensal responses are observed as early as 3 mo after birth, suggesting that both isotypes are induced during initial gut colonization by healthy microbiota.

Materials and methods

Human specimens

Surgical samples from histologically normal ascending colon were obtained from colon cancer patients (Table S2) undergoing hemicolectomy (Department of Surgery, Pitié-Salpêtrière Hospital, Paris, France). Patients with a history of intestinal inflammation were excluded from the study. Ileostomy fluids were collected from intensive care unit patients (Table S2). Fresh stool and blood samples were collected from 20 healthy volunteers (Fadlallah et al., 2018). Fresh stools from three IgA deficient patients with undetectable serum IgA levels (<0.07 mg/ml) were obtained from the Department of Clinical Immunology at Saint-Louis Hospital, Paris (Fadlallah et al., 2018). Antibiotic therapy or diarrhea in the last 3 mo were exclusion criteria in all instances. Maternal milk was obtained from three healthy donors. Stool samples, maternal milk, and plasma were immediately frozen after collection and stored at −80°C until use. All individuals signed a written consent and the protocol was approved by the local ethical committee of the Pitié-Salpêtrière Hospital.

Stool processing and microbiota purification

Fresh feces were aliquoted in a CO_2-rich/O_2-low atmosphere and stored at −80°C. Then microbiota were isolated by gradient purification under anaerobic conditions, as previously described (Juste et al., 2014). In brief, a density gradient of Nycodenz solution was prepared. Then, thawed stool was diluted in 1X-PBS (Eurobio), 60% Nycodenz, and 0.03% sodium deoxycholate and loaded on the gradient. After ultracentrifugation (45 min, 14,567 ×*g*, 4°C; Beckman Coulter ultracentrifuge), fecal bacteria were extracted and washed three times in 1X-PBS and 0.03% sodium deoxycholate and centrifuged. The final bacterial pellet was diluted in 1X-PBS-10% glycerol, immediately frozen in liquid nitrogen, and stored at −80°C.

Bacterial strains and culture conditions

Staphylococcus epidermidis, *S. aureus*, and *S. haemolyticus* were isolated from human stool samples and identified by Matrix Assisted Laser Desorption Ionization–Time of Flight (MALDI-TOF) mass spectrometry (Microbiology department, Pitié Salpêtrière Hospital, Paris). *B. longum* (E194v variant A) and *B. vulgatus* (NCTC11154) were collected and characterized at the Institut National de Recherche Agronomique (Jouy en Josas, France). Bacterial strains were cultured on sheep red blood agar plates at 37°C under aerobic (*Staphylococcus* sp., for 24 h) or anaerobic (*B. vulgatus* for 24 h and *B. longum* for 48 h) conditions. Individual colonies were picked, suspended in 1X-PBS-10X glycerol (10^9 CFU/ml), and frozen at −80°C. Quantification of CFUs was performed by adding counting beads (Beckman Coulter) to bacterial suspensions on a flow cytometer (FACS Canto II; BD Biosciences).

Production of human mAbs

For IgA production from long-term clonal B cell cultures, B cells were isolated from colonic lamina propria, dissected into 2-mm pieces, digested by the addition of collagenase in 1X-PBS (50 mg/ml; Roche), and then incubated at 37°C for 40 min. Lymphocytes were purified by centrifugation over Ficoll 400 (Eurobio) and stained with the following antibodies: anti-CD45 APC-H7, anti-CD19 BV421, anti-IgD FITC, anti-IgM BV605, anti-CD27 PE-Cy7 (all purchased from BD Biosciences), and anti-IgA PE (Jackson ImmunoResearch). Dead cells were excluded with LIVE/DEAD Fixable Aqua Dead Cell Stain Kit (Invitrogen). $CD45^+CD19^+CD27^+IgD^-IgM^-IgA^+$ B cells were sorted on a FACS Aria II cytometer (BD Biosciences). B cells were cultured for 4 d in the presence of irradiated (50 Gy) mouse fibroblasts expressing CD40L at a concentration of 10^4 cells per well (Arpin et al., 1995) and recombinant IL-21 (50 ng/ml, a kind gift of Dr. Arjen Bakker, AIMM Therapeutics, Amsterdam, Netherlands) in IMDM (Life Technologies), containing 10% FCS (Biowest) in a 96-well flat bottom plate. Retroviral transduction was performed with a Bcl-6– and Bcl-xL–expressing retroviral construct (AIMM Therapeutics) using experimental conditions described previously (Kwakkenbos et al., 2010). Briefly, activated B cells were incubated with retroviral supernatant and polybrene (final concentration, 4 µg/ml; Sigma-Aldrich) in a 96-well flat bottom plate, coated with the recombinant human fibronectin fragment CH-296 (Takara) for 8 h at 37°C. After washing, the cells were cultured for 4 d in the presence of irradiated CD40L-expressing mouse fibroblasts and recombinant IL-21 (50 ng/ml) in IMDM-10% FCS in 96-well flat bottom plates. Transduction efficiency based on GFP expression was monitored at day 4. B cells clones were then obtained by limiting dilution cultures, and IgAs were concentrated from culture supernatants with Amicon centrifugal filters (Millipore).

Human mAbs obtained through single-cell PCR processing of isolated IgA-producing colonic lamina propria B cells expressed variable IgA domains fused to human IgG1 constant domains in HEK293T cells, as previously described (Benckert et al., 2011).

Ig gene sequence analysis

RNA extracted from B cell lines (Trizol; Ambion) was reverse transcribed using random primers and SuperScript III (Invitrogen). Oligonucleotides used for VH and VL PCR are described in Table S3. Purified PCR products (GeneJET PCR Purification kit; Thermo Fisher Scientific) were sequenced (ABI Prism 3730) and analyzed using the ImMunoGeneTics information system (http://www.imgt.org). Frequencies of nonsilent to silent mutations in CDR1-CDR2 and FWR1-FWR3 were calculated for the *IGH* chain gene based on the total number of nucleotides analyzed.

Bacterial flow cytometry

mAb binding to microbiota was assessed by bacterial flow cytometry assay, as previously described (Moor et al., 2016). All buffers were passed through sterile 0.22-µm filters before use. Briefly, thawed microbiota or bacterial strains (10^6/condition) were fixed in 500 µl paraformaldehyde (4% in 1X-PBS) and stained with Cell Proliferation Dye eFluor 450 (eBioscience) for 25 min at 4°C. After washing with 1X-PBS (10 min, 4,000 ×*g*, 4°C), bacteria were suspended in 1X-PBS, 2% BSA (Sigma-Aldrich), 0.02% sodium azide (Sigma-Aldrich) in a 96-well V-bottom plate. mAb or human monoclonal anti-TNP IgA (a kind gift of Dr Jönsson, Institut Pasteur, Paris, France) was added in a 96-well V-bottom plate at a final concentration of 1 µg/ml, and the plates were incubated for 30 min at 4°C. After washing, goat anti-human IgA FITC (1/400) or isotype control (both from Jackson ImmunoResearch) were incubated for 20 min at 4°C. mAbs bearing an IgG-Fc portion were detected with goat anti-human IgG-A647 (1/400; Jackson ImmunoResearch). Quantification of in vivo IgA1 and IgA2 binding was performed in the same way. Fixed microbiota were incubated with mouse anti-human IgA1-FITC and mouse anti-human IgA2 Alexa Fluor 647 (Southern Biotech) or isotype controls for 20 min at 4°C. For IgA1 and IgA2 binding to pure bacterial strains, purified IgA from breast milk (final concentration, 10 µg/ml) was added to 10^6 CFU of *B. vulgatus* and *B. longum* for 30 min at 4°C before the addition of anti-IgA1 and anti-IgA2 secondary antibodies. Then, bacteria were washed and resuspended in sterile PBS. Samples were run using a BD FACS Canto II, and 30,000 bacterial events were acquired. Analysis was performed with FlowJo software (Tree Star). Medians of fluorescence were used to measure mAb-binding levels for pure strains.

The same procedure was performed to assess the role of glycans in mAb binding to microbiota. Prior to fixation, thawed microbiota (10^6 bacteria/condition) were incubated with a cocktail of enzymes (PNGase F, Endo-O-glycosidase, α-2(3,6,8,9)-Neuraminidase, β(1,4)-Galactosidase, β-N-Acetylglycosaminidase) that remove N- and O-linked carbohydrates for 1h30 at 37°C, according to manufacturer's recommendations (Enzymatic Protein Deglycosylation Kit; Sigma-Aldrich). After washing in 1X-PBS, microbiota was stained as described above.

Sorting of IgA-bound microbiota

Gut microbiota obtained from an IgA-deficient patient was incubated with purified mAbs (final concentration, 1 µg/ml) in a 96-well V-bottom plate (10^7 bacteria/well, 10 wells/mAb) for 30 min at 4°C. After washing with 1X-PBS (10 min, 4,000 ×*g*, 4°C), cells were stained with goat anti-human IgA-FITC (1/200) or isotype control antibody (Jackson ImmunoResearch). For sorting of in vivo IgA1- or IgA2-bound commensal bacteria, purified fecal microbiota from five healthy donors were thawed, washed, and directly stained with mouse anti-human IgA1-FITC or mouse anti-human IgA2 Alexa Fluor 647 (Southern Biotech) in a 96-well V-bottom plate (10^7 bacteria/well, five wells/subclass) for 20 min at 4°C. After washing, sorting was performed using a microbiota-dedicated single laser S3 cell sorter (Bio-Rad). Of note, while flow cytometry analysis is performed on fixed samples, combined flow sorting and DNA sequencing is performed on live bacteria in order to allow unbiased and optimal DNA extraction. Sorted bacteria (9.10^5) were collected in 1X-PBS at 4°C, centrifuged (8,000 ×*g*, 10 min, 4°C), and stored at −80°C until DNA extraction. Purity for both fractions was systematically verified after sorting. To check the absence of contaminants in flow cytometer fluid lines, sheath fluid was regularly incubated in Brain-Heart Infusion Broth (BioMérieux) at 37°C for 7 d.

16S rRNA gene sequencing and analysis

DNA was extracted using Trizol (Ambion), according to the manufacturer's instructions. Amplicons of V3-V4 regions of 16S rRNA genes were generated in a PCR mix containing 5 µl of extracted DNA, 500 U MolTaq 16S (Molzym), 10 mM dNTP (Invitrogen), and 10 pmol/µl V3-external and V4-external primers (Table S3) in MolTaq buffer (Molzym) diluted in DNA-free water (Molzym) for a final volume of 50 µl. 2 µl of first-round PCR reaction (initial denaturation 95°C 10 min, 95°C 1 min, 54°C 1 min, and 72°C 1 min, 10 times, final extension 72°C 10 min) was used as template in a second-round PCR (initial denaturation 95°C 10 min, 95°C 1 min, 66°C 1 min, 72°C 1 min, 10 times, final extension 72°C 10 min) with V3-V4 barcoded primers (Table S3). PCR products were purified using paramagnetic beads (Agencourt Ampure XP; Beckman Coulter) and sequenced on a MiSeq instrument (Illumina) in a multiplexed sequencing run (paired-end 250-nt reads) at the iGenSeq ICM facility (Institut du Cerveau et de la Moelle Epinière, Paris, France).

Demultiplexed reads were processed using the MG-RAST analysis pipeline. Sequencing artifacts, host DNA contamination, and sequences <200 bp in length were removed. Insufficient-quality reads were discarded (<5% of total reads). Sequences were then clustered into operational taxonomic units (OTUs) with a 97% homology using Greengenes database. OTUs containing only a single sequence were discarded. Previously published contaminant sequences (Salter et al., 2014) were removed if present in only one sorted fraction and absent from paired fractions. OTUs detected at >0.1% relative abundance in at least two samples were finally conserved. This process reduced the total OTU count from 313 down to 178. The OTU table was rarefied to the minimum sample's depth (5,000 reads). The Shannon index was calculated according to the following equation: Shannon index = $-\ \Sigma\ p_i\ ln(p_i)$, where p_i is the relative abundance of the *i*th OTU in the dataset. In calculating the EI, we scored a pseudorelative abundance equal to 0.0001, which was

the lower limit of detection, if a taxon was not detected in a given fraction. Specificity of IgA1$^+$IgA2$^+$ targeting was calculated using the following formula: $\frac{Number\ of\ samples\ in\ which\ OTU\ had\ a\ positive\ IgA1IgA2\ EI}{Number\ of\ samples}$, while specificity of IgA2$^+$ targeting was calculated with the formula: $\frac{Number\ of\ samples\ in\ which\ OTU\ had\ a\ negative\ IgA1IgA2\ EI}{Number\ of\ samples}$, in which IgA1IgA2 EI refers to $log10\left(\frac{IgA1+IgA2+taxon\ abundance}{IgA2+taxon\ abundance}\right)$.

Purification and quantification of IgA

Breast milk was centrifuged at 4,000 ×*g* for 10 min to remove the fat content. Aqueous phase was diluted in PBS to achieve pH 7.0 and filtered through a 0.22-µm syringe filter. The breast milk suspension was loaded onto peptide M/agarose gravity flow column (InvivoGen) at a flow rate of 0.5 ml/min. The column was washed with 20 column volumes of 1X-PBS. IgA was then eluted with 10 ml of 0.1 M glycine (pH 2–3; Sigma-Aldrich) and immediately neutralized to pH 7.5 with 1 M Tris (pH 8.5; Sigma-Aldrich). Buffer exchange was performed by filtration through a 100-kD membrane (Millipore). For free fecal IgA purification, fecal water were centrifuged twice at 13,000 ×*g* for 20 min at 4°C to eliminate debris and contaminants. After 0.22-µm filtration, IgA was isolated from fecal water as breast milk. Because the IgA concentration is low in fecal water, the sample was loaded three times onto the column to increase efficiency.

For IgA1 and IgA2 purification, serum from five healthy donors was pooled and diluted in 1X-PBS (IgA final concentration, 0.5–1 mg/ml). First, IgA was isolated with a peptide M/agarose column using the same process as that for breast milk. Then, purified IgA was loaded onto an immobilized Jacalin column (Thermo Fisher Scientific). The column was washed with 10 column volumes of PBS; this fraction contained IgA2. The column was washed again with PBS until absorbance at 280 nm reached the baseline (Nanovue; GE Healthcare), and 0.1 M α-D-galactose (Sigma-Aldrich) was added to the column to recover the bound IgA1. Buffer exchange was performed to remove galactose from IgA1 and to concentrate IgA2 with a 100-kD ultrafiltration membrane (Millipore). The purity of the IgA1 and IgA2 fractions was assessed by ELISA. These antibody solutions were divided into aliquots and frozen at −20°C.

The quantification of IgA in culture supernatants or after purification was determined using an ELISA quantitation set (Bethyl), according to the manufacturer's recommendations.

ELISA

Endocab human IgA kit (Hycult; Biotech) was used to detect LPS reactivity of mAbs at 0.1 and 1 µg/ml. The experimental procedure followed the manufacturer's recommendations.

500 ng lipoteichoic acid from *S. aureus* (Sigma-Aldrich) was coated onto 96-well Nunc Maxisorp plate (Thermo Fisher Scientific) overnight. Free sites were blocked with 1X-PBS, 1% BSA for 30 min at room temperature. mAbs were incubated for 2 h at room temperature at 0.1 and 1 µg/ml. After five washes, HRP anti-human IgA (Bethyl) was added for 1 h, followed by 3,3′,5,5′ Tetramethylbenzidine substrate revealing reaction (Thermo Fisher Scientific). Absorbance was measured at 450 nm.

Indirect immunofluorescence assay

HEp-2000 slides (ImmunoConcepts) were incubated with 25 µl mAb at 2 µg/ml for 25 min in a moist chamber at room temperature. A serum containing IgA anti-DNA served as a positive control and an irrelevant mAb culture supernatant as a negative control in all experiments. After washing with PBS, anti-human IgA FITC (Inova Diagnostics) was added for 25 min in a moist chamber at room temperature. After washing, fluorescence patterns were immediately detected with a fluorescent microscope (Leica).

Glycan microarray analysis

Glycan microarray screening using Consortium for Functional Glycomics (CFG) version 5.3 slides or from Semiotik was performed as previously described (Schneider et al., 2015; von Gunten et al., 2009; Stowell et al., 2014). The CFG microarray screening was performed at the National Center for Functional Glycomics at Beth Israel Deaconess Medical Center (Boston, MA). Scanning of Semiotik slides was performed on a ScanRI Microarray Scanner (PerkinElmer) with 5 µm resolution. The CFG glycan array data are published on the CFG website (http://www.functionalglycomics.org/glycomics/publicdata/primaryscreen.jsp). mAbs were diluted in PBS and screened at 10 µg/ml, if not stated otherwise; polyclonal IgA preparations were diluted in PBS and screened at 200 µg/ml. Commercially available secretory component (Labforce) was diluted in PBS and screened at 50 µg/ml. Commercially available human myeloma IgA2 (400110; Sigma-Aldrich) or mAb was used as a control. For the analysis of the CFG slides, the 90th percentile was used to indicate glycan significantly bound by IgA. For the analysis of the Semiotik slides, per recommendation of the manufacturer, RFU values five times higher than the empty spot negative control were considered positive. The computed ABR is representative of the quotient of the respective sample RFU and the corresponding IgA control (Schneider et al., 2015; von Gunten et al., 2009). ABR intensities lower or equal to one were defined as unspecific binding. For purposes of analysis, ABR values lower than one were set to one. To assess preferential recognition by IgA1 or IgA2, the log10 (IgA2/IgA1) was calculated. Glycans showing values less than −0.2 was characterized as being preferentially recognized by IgA1, while values >0.2 were characterized as being preferentially recognized by IgA2 and values equal to or in between −0.2 and 0.2 were considered as showing no preferential reactivity.

PG and TA purification and dot blot assay

500 ml of overnight culture of *S. aureus* or *S. haemolyticus* was centrifuged. The pellet was suspended and centrifuged twice in 40 ml 50 mM TrisHCl, pH 7.4, 150 mM NaCl, and 1% SDS and boiled for 10 min. The resulting pellet was suspended in 40 ml 50 mM Tris, pH 7.4, and then sonicated and centrifuged. The resulting pellet was again treated in 40 ml 50 mM TrisHCl, pH 7.4, 150 mM NaCl, and 1% SDS and boiled for 10 min. PG-TA was then further purified to eliminate all other known contaminants by the following successive treatments: digestion with DNase (1 mg/ml) and RNase (5 mg/ml) in $MgSO_4$ 20 mM followed by a trypsin (10 mg/ml) digestion after addition of $CaCl_2$ (10 mM) for

12 h The resulting suspension was boiled for 10 min in 1% SDS and centrifuged. The pellet was then suspended and centrifuged in (1) H_2O, (2) 8 M $LiCl_2$, (3) 100 mM EDTA, (4) H_2O (twice), (5) 46% hydrofluoric acid, and finally (6) H_2O. TA was recovered from the hydrofluoric acid supernatant after evaporation.

20 µg of purified PG and TA from *S. aureus* and *S. haemolyticus* was coated on a nitrocellulose membrane (Bio-Rad). The membrane was blocked in 1X-PBS, 5% non-fat milk for 30 min at room temperature and washed in 1X-PBS, 0.05% Tween 20. mAbs were then incubated for 30 min at room temperature at 2 µg/ml. After washing, mAbs were detected with HRP-conjugated goat anti-human IgG used at 1:40,000 (A0170; Sigma-Aldrich), followed by enhanced chemiluminescence revealing reaction (Clarity Western ECL; Bio-Rad). All incubations were in 1X-PBS with 5% nonfat milk and washing steps in 1X-PBS with 0.05% Tween.

Functional cellular assays

Peripheral blood mononuclear cells were isolated from blood samples by density gradient centrifugation over Ficoll-Paque (Eurobio). Monocytes for macrophage differentiation were isolated by plastic adherence as follows: peripheral blood mononuclear cells were distributed into a 25-cm^2 flask and allowed to adhere for 1 h at 37°C in RPMI (Gibco) supplemented with 10% FCS (Biowest). Nonadherent cells were removed, and the adherent monocytes were washed twice with medium, detached with Versene (Invitrogen), counted, seeded in 96-well U-bottom plates at a density of 5.10^4 cells/well, and cultured in RPMI-10% FCS in the presence of 100 ng/ml human GM-CSF (Miltenyi Biotec) in a total volume of 100 µl. At day 6, macrophages were stimulated with 5.10^5 *S. aureus,* which had been preincubated with 0.5 mg/ml of purified IgA1 or IgA2 and washed. After 24 h, cytokine levels in supernatants were measured using the Cytokine 3-Plex A (IL-6, IL-10, and TNF-α) immunoassay (Quanterix) relying on a Single Molecule Array (Simoa) technology run on a HD-1 Analyzer (Quanterix). Working dilutions were 1:500 in diluent sample. The lower limits of quantification for IL-6, IL-10, and TNF-α were 5.5, 3.65, and 25.5 pg/ml, respectively.

Statistical analysis

Statistical analysis was performed using GraphPad Prism version 6. Nonparametric tests were used whenever necessary; a Wilcoxon paired rank test was used when comparing paired groups, a Mann-Whitney test when comparing two independent groups, and a Kruskal-Wallis test for multiple comparisons. Significant P values ($P < 0.05$) are indicated on plots (*, $P < 0.05$; **, $P < 0.01$; ***, $P < 0.001$). Hierarchical clustering algorithms were run with Partek software or "R" (The R Foundation for Statistical Computing, version 3.4.3).

Online supplemental material

Fig. S1 presents the secretory component glycan-binding pattern and additional characterization of gut-derived IgA reactivity. Fig. S2 further explores interindividual microbiota variability. Fig. S3 presents milk-derived IgA reactivity and functional assays. Fig. S4 shows additional characterization of monoclonal-binding patterns. Fig. S5 describes monoclonal self-reactivity. Table S1 presents Ig gene sequence analysis of dimeric antibodies. Table S2 lists additional demographic data of human specimens used in this study. Table S3 lists primers used for Ig and 16S rDNA gene amplification.

Acknowledgments

The authors thank Dr. Hergen Spits and Arjen Bakker (AIMM Therapeutics, Amsterdam, Netherlands) for the kind gift of the Bcl-6/Bcl-xL–expressing retrovirus and reagents. The authors also thank Nijas Aliu (Department of Pediatrics, Inselspital, Bern University Hospital, Bern, Switzerland) and Julia Gärtner (Division of B Cell Immunology, German Cancer Research Center, Heidelberg, Germany) for technical assistance.

D. Sterlin was partially supported for this work by a Pasteur/Assistance Publique Hôpitaux de Paris interface fellowship, and J. Fadlallah was supported by the Institut national de la santé et de la recherche médicale Poste d'accueil fellowship. The study was financed by Institut national de la santé et de la recherche médicale and Agence Nationale de la Recherche (MetAntibody; grant ANR-14-CE14-0013 to M. Larsen). Research in the laboratory of S. von Gunten is supported by the Swiss National Science Foundation (grants 310030_184757 and 310030_162552) and the Swiss Cancer League/Swiss Cancer Research (grant KFS-3941-08-2016).

Author contributions: J. Fadlallah, C. Capito, C. Fieschi, H. Brisson, and C. Tresallet recruited patients. D. Sterlin, J. Fadlallah, C. Juste, and M. Larsen prepared the specimens from healthy donors. A. Aubry and F. Jönsson provided bacterial strains or control antibodies. H. Wardemann provided previously characterized monomeric human IgA clones bearing the IgG1 Fc portion. D. Sterlin, J. Fadlallah, C. Parizot, K. Dorgham, A. Rajkumar, G. Autaa, J.L. Charuel, F. Jönsson, and T. Candela designed and performed experiments. D. Sterlin, J. Fadlallah, O. Adams, and H. El-Kafsi performed data analysis. R.D. Cummings supervised glycan microarray analysis and reviewed the manuscript. D. Sterlin, O. Adams, H. Yssel, S. von Gunten, and G. Gorochov designed the study, prepared the figures, and wrote the manuscript.

Disclosures: Drs. Sterlin, Fadlallah, Larsen, and Gorochov reported a patent to EP 18306006.0 pending. No other disclosures were reported.;

Submitted: 24 August 2018
Revised: 10 May 2019
Accepted: 22 November 2019

References

Aleyd, E., M.H. Heineke, and M. van Egmond. 2015. The era of the immunoglobulin A Fc receptor FcαRI; its function and potential as target in disease. *Immunol. Rev.* 268:123–138. https://doi.org/10.1111/imr.12337

Arbatsky, N.P., A.S. Shashkov, E. Literacka, G. Widmalm, W. Kaca, and Y.A. Knirel. 2000. Structure of the O-specific polysaccharide of Proteus mirabilis O11, another Proteus O-antigen containing an amide of D-galacturonic acid with L-threonine. *Carbohydr. Res.* 323:81–86. https://doi.org/10.1016/S0008-6215(99)00257-8

Arpin, C., J. Déchanet, C. Van Kooten, P. Merville, G. Grouard, F. Brière, J. Banchereau, and Y.J. Liu. 1995. Generation of memory B cells and plasma cells in vitro. *Science.* 268:720–722. https://doi.org/10.1126/science.7537388

Balu, S., R. Reljic, M.J. Lewis, R.J. Pleass, R. McIntosh, C. van Kooten, M. van Egmond, S. Challacombe, J.M. Woof, and J. Ivanyi. 2011. A novel human IgA monoclonal antibody protects against tuberculosis. *J. Immunol.* 186: 3113–3119. https://doi.org/10.4049/jimmunol.1003189

Bastos, P.A.D., J.P. da Costa, and R. Vitorino. 2017. A glimpse into the modulation of post-translational modifications of human-colonizing bacteria. *J. Proteomics.* 152:254–275. https://doi.org/10.1016/j.jprot.2016.11.005

Benckert, J., N. Schmolka, C. Kreschel, M.J. Zoller, A. Sturm, B. Wiedenmann, and H. Wardemann. 2011. The majority of intestinal IgA+ and IgG+ plasmablasts in the human gut are antigen-specific. *J. Clin. Invest.* 121: 1946–1955. https://doi.org/10.1172/JCI44447

Berkowska, M.A., G.J.A. Driessen, V. Bikos, C. Grosserichter-Wagener, K. Stamatopoulos, A. Cerutti, B. He, K. Biermann, J.F. Lange, M. van der Burg, et al. 2011. Human memory B cells originate from three distinct germinal center-dependent and -independent maturation pathways. *Blood.* 118:2150–2158. https://doi.org/10.1182/blood-2011-04-345579

Berkowska, M.A., J.-N. Schickel, C. Grosserichter-Wagener, D. de Ridder, Y.S. Ng, J.J.M. van Dongen, E. Meffre, and M.C. van Zelm. 2015. Circulating Human CD27-IgA+ Memory B Cells Recognize Bacteria with Polyreactive Igs. *J. Immunol.* 195:1417–1426. https://doi.org/10.4049/jimmunol.1402708

Bunker, J.J., T.M. Flynn, J.C. Koval, D.G. Shaw, M. Meisel, B.D. McDonald, I.E. Ishizuka, A.L. Dent, P.C. Wilson, B. Jabri, et al. 2015. Innate and Adaptive Humoral Responses Coat Distinct Commensal Bacteria with Immunoglobulin A. *Immunity.* 43:541–553. https://doi.org/10.1016/j.immuni.2015.08.007

Bunker, J.J., S.A. Erickson, T.M. Flynn, C. Henry, J.C. Koval, M. Meisel, B. Jabri, D.A. Antonopoulos, P.C. Wilson, and A. Bendelac. 2017. Natural polyreactive IgA antibodies coat the intestinal microbiota. *Science.* 358: eaan6619. https://doi.org/10.1126/science.aan6619

Butler, C.A., P.D. Veith, M.F. Nieto, S.G. Dashper, and E.C. Reynolds. 2015. Lysine acetylation is a common post-translational modification of key metabolic pathway enzymes of the anaerobe Porphyromonas gingivalis. *J. Proteomics.* 128:352–364. https://doi.org/10.1016/j.jprot.2015.08.015

Bystrova, O.V., G.V. Zatonskii, S.A. Borisova, N.A. Kocharova, A.S. Shashkov, Y.A. Knirel, E.V. Kholodkova, and E.S. Stanislavskii. 2000. Structure of an acidic O-specific polysaccharide of the bacterium Providencia alcalifaciens O7. *Biochemistry (Mosc.).* 65:677–684.

Chiba, M., H. Ohta, H. Yagisawa, and O. Masamune. 1987. IgA1 & IgA2 distribution in the intestine. *Gastroenterol. Jpn.* 22:18–23. https://doi.org/10.1007/BF02806330

Coffman, R.L., D.A. Lebman, and B. Shrader. 1989. Transforming growth factor beta specifically enhances IgA production by lipopolysaccharide-stimulated murine B lymphocytes. *J. Exp. Med.* 170:1039–1044. https://doi.org/10.1084/jem.170.3.1039

D'Auria, G., F. Peris-Bondia, M. Džunková, A. Mira, M.C. Collado, A. Latorre, and A. Moya. 2013. Active and secreted IgA-coated bacterial fractions from the human gut reveal an under-represented microbiota core. *Sci. Rep.* 3:3515. https://doi.org/10.1038/srep03515

Donaldson, G.P., S.M. Lee, and S.K. Mazmanian. 2016. Gut biogeography of the bacterial microbiota. *Nat. Rev. Microbiol.* 14:20–32. https://doi.org/10.1038/nrmicro3552

Fadlallah, J., H. El Kafsi, D. Sterlin, C. Juste, C. Parizot, K. Dorgham, G. Autaa, D. Gouas, M. Almeida, P. Lepage, et al. 2018. Microbial ecology perturbation in human IgA deficiency. *Sci. Transl. Med.* 10:eaan1217. https://doi.org/10.1126/scitranslmed.aan1217

Forbes, S.J., M. Eschmann, and N.J. Mantis. 2008. Inhibition of Salmonella enterica serovar typhimurium motility and entry into epithelial cells by a protective antilipopolysaccharide monoclonal immunoglobulin A antibody. *Infect. Immun.* 76:4137–4144. https://doi.org/10.1128/IAI.00416-08

Forbes, S.J., T. Bumpus, E.A. McCarthy, B. Corthésy, and N.J. Mantis. 2011. Transient suppression of Shigella flexneri type 3 secretion by a protective O-antigen-specific monoclonal IgA. *MBio.* 2:e00042–e11. https://doi.org/10.1128/mBio.00042-11

Grangeasse, C., J. Stülke, and I. Mijakovic. 2015. Regulatory potential of post-translational modifications in bacteria. *Front. Microbiol.* 6:500. https://doi.org/10.3389/fmicb.2015.00500

Griesemer, A., K. Yamada, and M. Sykes. 2014. Xenotransplantation: immunological hurdles and progress toward tolerance. *Immunol. Rev.* 258: 241–258. https://doi.org/10.1111/imr.12152

Hansen, I.S., W. Hoepel, S.A.J. Zaat, D.L.P. Baeten, and J. den Dunnen. 2017. Serum IgA Immune Complexes Promote Proinflammatory Cytokine Production by Human Macrophages, Monocytes, and Kupffer Cells through FcαRI-TLR Cross-Talk. *J. Immunol.* 199:4124–4131. https://doi.org/10.4049/jimmunol.1700883

Harriman, G.R., M. Bogue, P. Rogers, M. Finegold, S. Pacheco, A. Bradley, Y. Zhang, and I.N. Mbawuike. 1999. Targeted deletion of the IgA constant region in mice leads to IgA deficiency with alterations in expression of other Ig isotypes. *J. Immunol.* 162:2521–2529.

He, B., W. Xu, P.A. Santini, A.D. Polydorides, A. Chiu, J. Estrella, M. Shan, A. Chadburn, V. Villanacci, A. Plebani, et al. 2007. Intestinal bacteria trigger T cell-independent immunoglobulin A(2) class switching by inducing epithelial-cell secretion of the cytokine APRIL. *Immunity.* 26: 812–826. https://doi.org/10.1016/j.immuni.2007.04.014

Hellwig, S.M., A.B. van Spriel, J.F. Schellekens, F.R. Mooi, and J.G. van de Winkel. 2001. Immunoglobulin A-mediated protection against Bordetella pertussis infection. *Infect. Immun.* 69:4846–4850. https://doi.org/10.1128/IAI.69.8.4846-4850.2001

Johansen, F.E., M. Pekna, I.N. Norderhaug, B. Haneberg, M.A. Hietala, P. Krajci, C. Betsholtz, and P. Brandtzaeg. 1999. Absence of epithelial immunoglobulin A transport, with increased mucosal leakiness, in polymeric immunoglobulin receptor/secretory component-deficient mice. *J. Exp. Med.* 190:915–922. https://doi.org/10.1084/jem.190.7.915

Juste, C., D.P. Kreil, C. Beauvallet, A. Guillot, S. Vaca, C. Carapito, S. Mondot, P. Sykacek, H. Sokol, F. Blon, et al. 2014. Bacterial protein signals are associated with Crohn's disease. *Gut.* 63:1566–1577. https://doi.org/10.1136/gutjnl-2012-303786

Kau, A.L., J.D. Planer, J. Liu, S. Rao, T. Yatsunenko, I. Trehan, M.J. Manary, T.-C. Liu, T.S. Stappenbeck, K.M. Maleta, et al. 2015. Functional characterization of IgA-targeted bacterial taxa from undernourished Malawian children that produce diet-dependent enteropathy. *Sci. Transl. Med.* 7:276ra24. https://doi.org/10.1126/scitranslmed.aaa4877

Kawamoto, S., T.H. Tran, M. Maruya, K. Suzuki, Y. Doi, Y. Tsutsui, L.M. Kato, and S. Fagarasan. 2012. The inhibitory receptor PD-1 regulates IgA selection and bacterial composition in the gut. *Science.* 336:485–489. https://doi.org/10.1126/science.1217718

Kwakkenbos, M.J., S.A. Diehl, E. Yasuda, A.Q. Bakker, C.M.M. van Geelen, M.V. Lukens, G.M. van Bleek, M.N. Widjojoatmodjo, W.M.J.M. Bogers, H. Mei, et al. 2010. Generation of stable monoclonal antibody-producing B cell receptor-positive human memory B cells by genetic programming. *Nat. Med.* 16:123–128. https://doi.org/10.1038/nm.2071

Ladjeva, I., J.H. Peterman, and J. Mestecky. 1989. IgA subclasses of human colostral antibodies specific for microbial and food antigens. *Clin. Exp. Immunol.* 78:85–90.

Lee, J., D.R. Boutz, V. Chromikova, M.G. Joyce, C. Vollmers, K. Leung, A.P. Horton, B.J. DeKosky, C.-H. Lee, J.J. Lavinder, et al. 2016. Molecular-level analysis of the serum antibody repertoire in young adults before and after seasonal influenza vaccination. *Nat. Med.* 22:1456–1464. https://doi.org/10.1038/nm.4224

Lindner, C., I. Thomsen, B. Wahl, M. Ugur, M.K. Sethi, M. Friedrichsen, A. Smoczek, S. Ott, U. Baumann, S. Suerbaum, et al. 2015. Diversification of memory B cells drives the continuous adaptation of secretory antibodies to gut microbiota. *Nat. Immunol.* 16:880–888. https://doi.org/10.1038/ni.3213

Ludvigsson, J.F., M. Neovius, and L. Hammarström. 2016. Risk of Infections Among 2100 Individuals with IgA Deficiency: a Nationwide Cohort Study. *J. Clin. Immunol.* 36:134–140. https://doi.org/10.1007/s10875-015-0230-9

Macek, B., F. Gnad, B. Soufi, C. Kumar, J.V. Olsen, I. Mijakovic, and M. Mann. 2008. Phosphoproteome analysis of E. coli reveals evolutionary conservation of bacterial Ser/Thr/Tyr phosphorylation. *Mol. Cell. Proteomics.* 7:299–307. https://doi.org/10.1074/mcp.M700311-MCP200

Magri, G., L. Comerma, M. Pybus, J. Sintes, D. Lligé, D. Segura-Garzón, S. Bascones, A. Yeste, E.K. Grasset, C. Gutzeit, et al. 2017. Human Secretory IgM Emerges from Plasma Cells Clonally Related to Gut Memory B Cells and Targets Highly Diverse Commensals. *Immunity.* 47: 118–134.e8. https://doi.org/10.1016/j.immuni.2017.06.013

Moor, K., J. Fadlallah, A. Toska, D. Sterlin, M.L. Balmer, A.J. Macpherson, G. Gorochov, M. Larsen, and E. Slack. 2016. Analysis of bacterial-surface-specific antibodies in body fluids using bacterial flow cytometry. *Nat. Protoc.* 11:1531–1553. https://doi.org/10.1038/nprot.2016.091

Moreau, M.C., R. Ducluzeau, D. Guy-Grand, and M.C. Muller. 1978. Increase in the population of duodenal immunoglobulin A plasmocytes in axenic mice associated with different living or dead bacterial strains of intestinal origin. *Infect. Immun.* 21:532–539.

Nakajima, A., A. Vogelzang, M. Maruya, M. Miyajima, M. Murata, A. Son, T. Kuwahara, T. Tsuruyama, S. Yamada, M. Matsuura, et al. 2018. IgA regulates the composition and metabolic function of gut microbiota by promoting symbiosis between bacteria. *J. Exp. Med.* 215:2019–2034. https://doi.org/10.1084/jem.20180427

Okai, S., F. Usui, S. Yokota, Y. Hori-I, M. Hasegawa, T. Nakamura, M. Kurosawa, S. Okada, K. Yamamoto, E. Nishiyama, et al. 2016. High-affinity monoclonal IgA regulates gut microbiota and prevents colitis in mice. *Nat. Microbiol.* 1:16103. https://doi.org/10.1038/nmicrobiol.2016.103

Pabst, O. 2012. New concepts in the generation and functions of IgA. *Nat. Rev. Immunol.* 12:821–832. https://doi.org/10.1038/nri3322

Pakkanen, S.H., J.M. Kantele, Z. Moldoveanu, S. Hedges, M. Häkkinen, J. Mestecky, and A. Kantele. 2010. Expression of homing receptors on IgA1 and IgA2 plasmablasts in blood reflects differential distribution of IgA1 and IgA2 in various body fluids. *Clin. Vaccine Immunol.* 17:393–401. https://doi.org/10.1128/CVI.00475-09

Palm, N.W., M.R. de Zoete, T.W. Cullen, N.A. Barry, J. Stefanowski, L. Hao, P.H. Degnan, J. Hu, I. Peter, W. Zhang, et al. 2014. Immunoglobulin A coating identifies colitogenic bacteria in inflammatory bowel disease. *Cell.* 158:1000–1010. https://doi.org/10.1016/j.cell.2014.08.006

Pasquier, B., P. Launay, Y. Kanamaru, I.C. Moura, S. Pfirsch, C. Ruffié, D. Hénin, M. Benhamou, M. Pretolani, U. Blank, and R.C. Monteiro. 2005. Identification of FcalphaRI as an inhibitory receptor that controls inflammation: dual role of FcRgamma ITAM. *Immunity.* 22:31–42. https://doi.org/10.1016/j.immuni.2004.11.017

Peterson, D.A., N.P. McNulty, J.L. Guruge, and J.I. Gordon. 2007. IgA response to symbiotic bacteria as a mediator of gut homeostasis. *Cell Host Microbe.* 2:328–339. https://doi.org/10.1016/j.chom.2007.09.013

Ribet, D., and P. Cossart. 2010. Pathogen-mediated posttranslational modifications: A re-emerging field. *Cell.* 143:694–702. https://doi.org/10.1016/j.cell.2010.11.019

Rollenske, T., V. Szijarto, J. Lukasiewicz, L.M. Guachalla, K. Stojkovic, K. Hartl, L. Stulik, S. Kocher, F. Lasitschka, M. Al-Saeedi, et al. 2018. Cross-specificity of protective human antibodies against Klebsiella pneumoniae LPS O-antigen. *Nat. Immunol.* 19:617–624. https://doi.org/10.1038/s41590-018-0106-2

Rossato, E., S. Ben Mkaddem, Y. Kanamaru, M. Hurtado-Nedelec, G. Hayem, V. Descatoire, C. Vonarburg, S. Miescher, A.W. Zuercher, and R.C. Monteiro. 2015. Reversal of Arthritis by Human Monomeric IgA Through the Receptor-Mediated SH2 Domain-Containing Phosphatase 1 Inhibitory Pathway. *Arthritis Rheumatol.* 67:1766–1777. https://doi.org/10.1002/art.39142

Salter, S.J., M.J. Cox, E.M. Turek, S.T. Calus, W.O. Cookson, M.F. Moffatt, P. Turner, J. Parkhill, N.J. Loman, and A.W. Walker. 2014. Reagent and laboratory contamination can critically impact sequence-based microbiome analyses. *BMC Biol.* 12:87. https://doi.org/10.1186/s12915-014-0087-z

Schauer, U., F. Stemberg, C.H.L. Rieger, M. Borte, S. Schubert, F. Riedel, U. Herz, H. Renz, M. Wick, and W. Herzog. 2003. Establishment of age-dependent reference values for IgA subclasses. *Clin. Chim. Acta.* 328:129–133. https://doi.org/10.1016/S0009-8981(02)00418-7

Schneider, C., D.F. Smith, R.D. Cummings, K.F. Boligan, R.G. Hamilton, B.S. Bochner, S. Miescher, H.-U. Simon, A. Pashov, T. Vassilev, and S. von Gunten. 2015. The human IgG anti-carbohydrate repertoire exhibits a universal architecture and contains specificity for microbial attachment sites. *Sci. Transl. Med.* 7:269ra1. https://doi.org/10.1126/scitranslmed.3010524

Sekirov, I., S.L. Russell, L.C.M. Antunes, and B.B. Finlay. 2010. Gut microbiota in health and disease. *Physiol. Rev.* 90:859–904. https://doi.org/10.1152/physrev.00045.2009

Stowell, S.R., C.M. Arthur, R. McBride, O. Berger, N. Razi, J. Heimburg-Molinaro, L.C. Rodrigues, J.-P. Gourdine, A.J. Noll, S. von Gunten, et al. 2014. Microbial glycan microarrays define key features of host-microbial interactions. *Nat. Chem. Biol.* 10:470–476. https://doi.org/10.1038/nchembio.1525

Sugahara, K., N.B. Schwartz, and A. Dorfman. 1979. Biosynthesis of hyaluronic acid by Streptococcus. *J. Biol. Chem.* 254:6252–6261.

Tsepilov, R.N., and A.V. Beloded. 2015. Hyaluronic Acid—an "Old" Molecule with "New" Functions: Biosynthesis and Depolymerization of Hyaluronic Acid in Bacteria and Vertebrate Tissues Including during Carcinogenesis. *Biochemistry (Mosc.).* 80:1093–1108. https://doi.org/10.1134/S0006297915090011

von Gunten, S., D.F. Smith, R.D. Cummings, S. Riedel, S. Miescher, A. Schaub, R.G. Hamilton, and B.S. Bochner. 2009. Intravenous immunoglobulin contains a broad repertoire of anticarbohydrate antibodies that is not restricted to the IgG2 subclass. *J. Allergy Clin. Immunol.* 123:1268–76.e15. https://doi.org/10.1016/j.jaci.2009.03.013

Wilmore, J.R., B.T. Gaudette, D. Gomez Atria, T. Hashemi, D.D. Jones, C.A. Gardner, S.D. Cole, A.M. Misic, D.P. Beiting, and D. Allman. 2018. Commensal Microbes Induce Serum IgA Responses that Protect against Polymicrobial Sepsis. *Cell Host Microbe.* 23:302–311.e3. https://doi.org/10.1016/j.chom.2018.01.005

Supplemental material

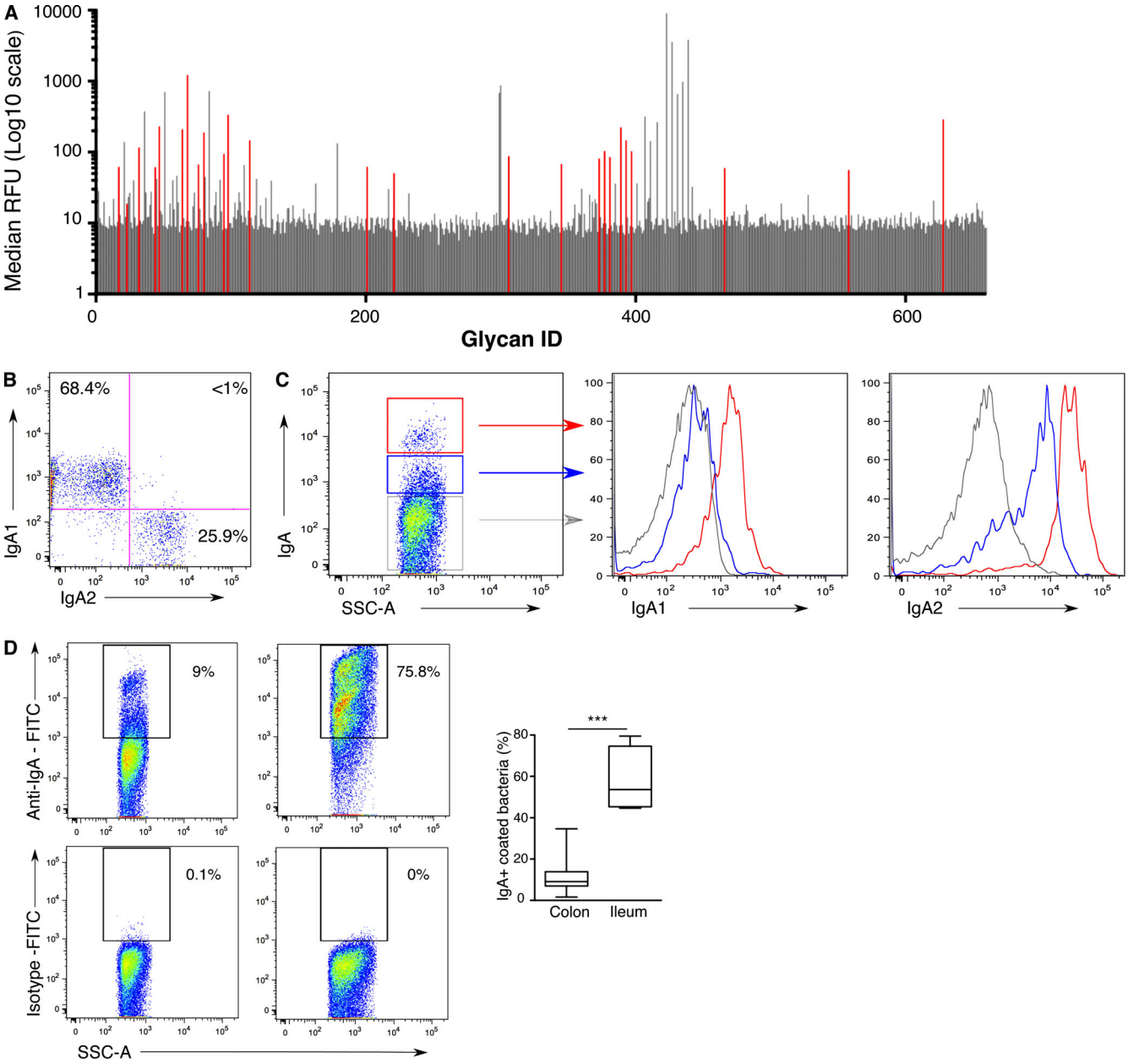

Figure S1. **Gut bacteria segregate into IgA^{bright} and IgA^{low} fractions in healthy humans.** Related to Figs. 1 and 2. **(A)** The secretory component binds a modest range of carbohydrates. Glycan reactivity with the secretory component was assessed using glycan microarray technology (660 structures). Representative median RFUs are shown. Glycans specifically recognized by secretory component are colored in red. **(B)** Anti-IgA1 and anti-IgA2 antibodies do not cross-react. Flow cytometry analysis of IgA1 and IgA2 expression on peripheral B cells from a healthy donor. **(C)** IgA-coated bacteria split into IgA^{bright} and IgA^{low} fractions depending on IgA1 and IgA2 coating. Representative flow cytometry analysis of IgA1 and IgA2 coating in IgA^{bright}-coated bacteria (red lines), IgA^{low}-coated bacteria (blue lines), and IgA-unbound bacteria (gray lines). **(D)** Representative flow cytometry analysis of human gut microbiota stained with anti-IgA FITC or isotype-matched control antibody (left and central panels). Numbers indicate percentage of positive cells. Data are cumulative from three independent experiments. Boxes extend from the 25th to the 75th percentiles. Error bars represent minimum and maximum values. P values were defined using the Mann-Whitney test. ***, P < 0.001. SSC-A, side scatter area. Quantification of IgA-coated bacteria in stool (n = 20) and ileum (n = 5).

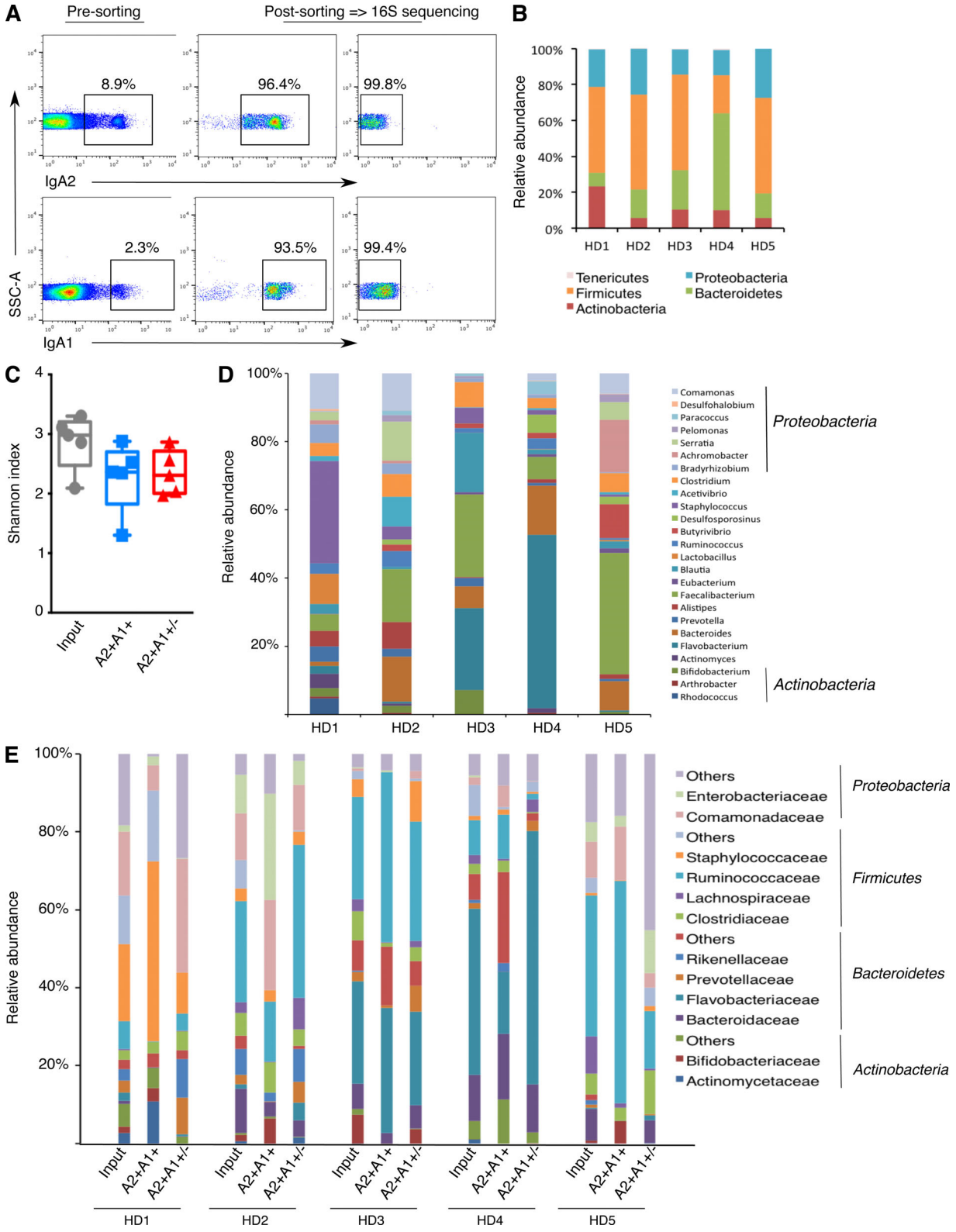

Figure S2. **IgA1⁺IgA2⁺- and IgA2⁺-sorted fractions show distinct compositions within the same donor and between donors.** Related to Fig. 4. **(A)** Sorting strategy of IgA1- and IgA2-coated bacteria (representative of five independent experiments). SSC-A, side scatter area. **(B)** Relative composition of phyla in fecal samples (input). Each column corresponds to one healthy donor (HD) sample out of five analysed (HD1 to HD5, as indicated). **(C)** Genera diversity of input, IgA1⁺, and IgA2⁺ fractions calculated using the Shannon index. Boxes extend from the 25th to the 75th percentiles. Error bars represent minimum and maximum values. **(D)** Relative composition of genera in fecal samples (input). Each column corresponds to one sample. The 25 most abundant genera are shown. **(E)** Relative abundance of families in input and sorted fractions from five healthy donors. The top 16 most abundant families are shown.

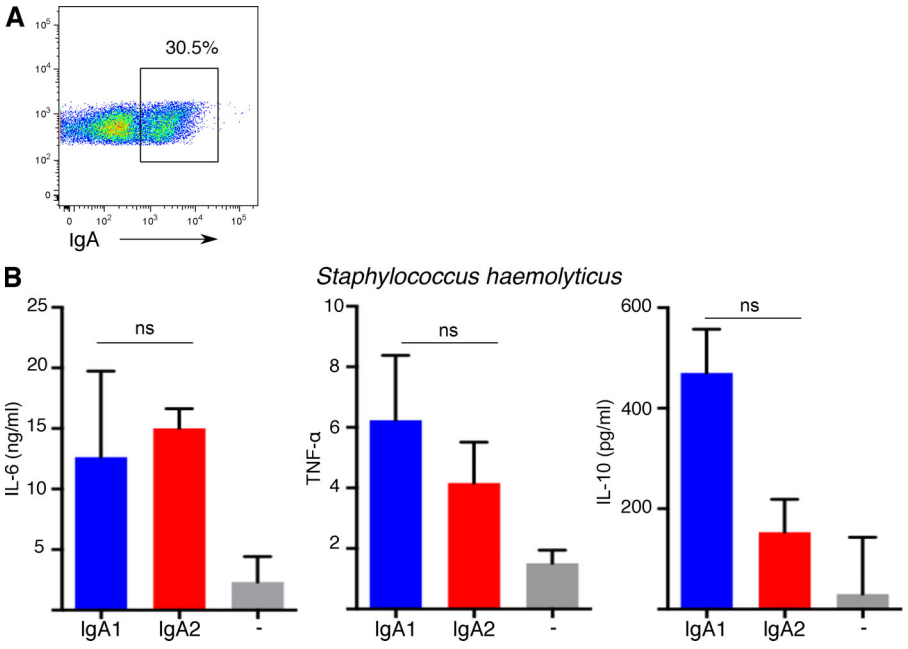

Figure S3. **IgA1- and IgA2-coated bacteria promote cytokine production by macrophages. (A)** One out of three representative flow cytometric analyses of human gut microbiota purified from an IgA-deficient donor incubated with breast milk IgA and subsequently with anti-IgA FITC (three independent experiments). Numbers indicate percentage of positive cells. **(B)** Cytokine levels measured using Simoa technology in supernatants of macrophages incubated for 24 h with heat-killed *S. haemolyticus* opsonized with IgA1 (blue) or IgA2 (red) or without IgA (gray). The Mann-Whitney test was used to calculate P values; ns, not significant (n = 3 healthy donors, two independent measurements). Error bars indicate maximum values.

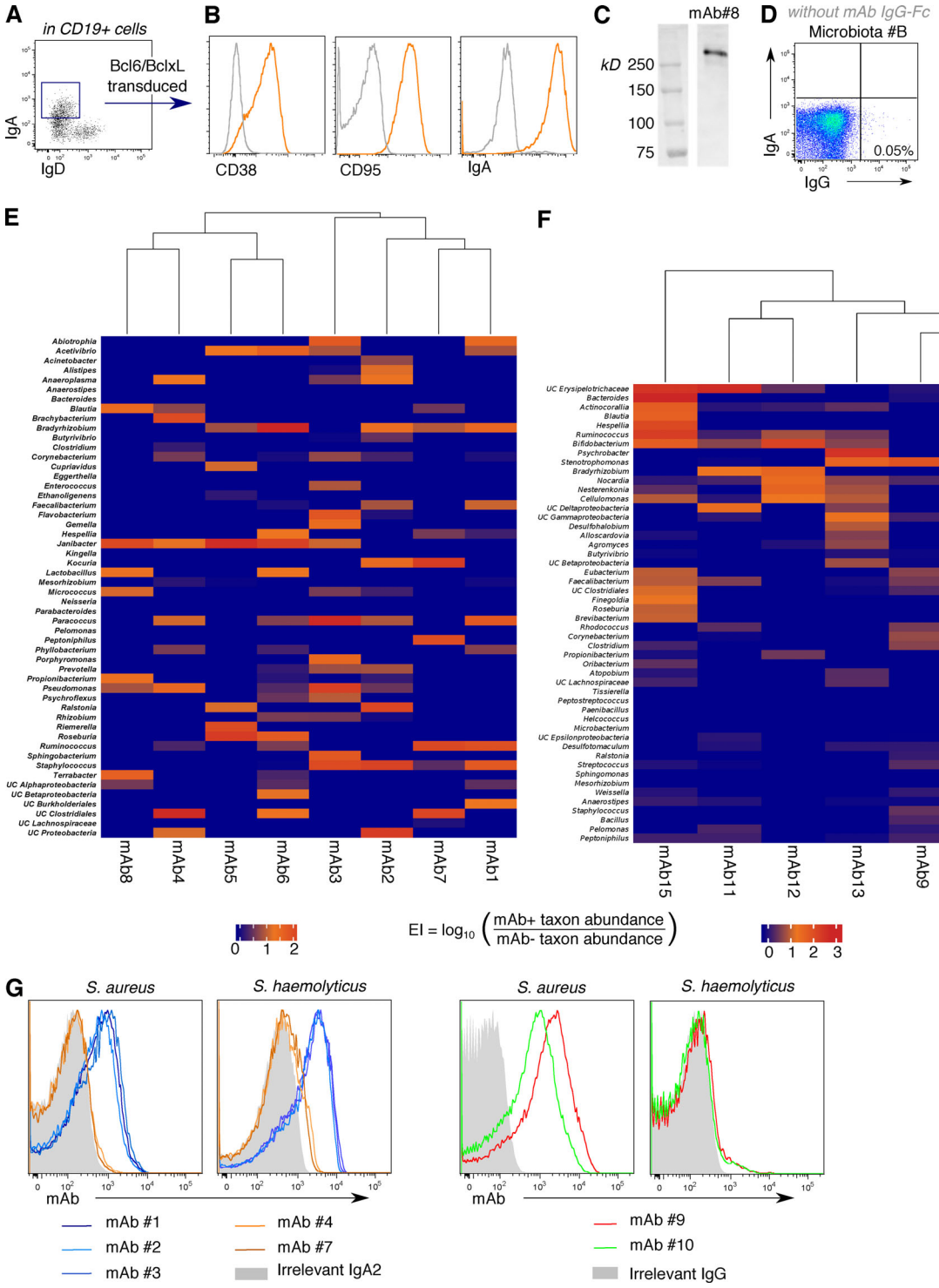

Figure S4. **Human monoclonal IgA bind a broad but nevertheless private pattern of commensals.** Related to Fig. 4. **(A)** Flow cytometric sorting of intestinal IgA$^+$ memory B cells (defined as CD19$^+$, cell surface IgA$^+$ IgD$^-$). Sort gate among CD19$^+$ B cells is shown. Doublets and dead cells were excluded before CD19 gating, CD19$^+$ cells were gated among CD45$^+$ cells (not shown). Representative images from three independent sorts are shown. **(B)** Transduced B cells exhibited a stable germinal center–like phenotype and maintained IgA expression. Transduced B cells were surface-labeled with anti-CD38, anti-CD95, or anti-IgA (orange lines) or appropriate isotype antibody controls (gray dotted lines). Representative images of eight monoclonal B cell lines, evaluated in three independent experiments, are shown. **(C)** Monoclonal B cell lines produced dimeric IgA. Representative immunoblotting showing high molecular weight dimeric mAb in nonreducing conditions for mAb 8. Representative image of eight mAbs and two independent experiments are shown. **(D)** Representative flow cytometric plot of microbiota B stained with anti-IgG Alexa Fluor 647 and anti-IgA FITC. The same experiment was repeated twice. **(E)** Heatmap diagram of EI of the 50 most frequent genera from microbiota A. Hierarchical clustering grouped mAb$^+$ fractions and genera. **(F)** Heatmap diagram of EI of the 50 most frequent genera from microbiota B. Hierarchical clustering grouped mAb$^+$ fractions and genera. **(G)** Flow cytometric analysis of mAb or negative control (mAb$^-$ supernatant [left] or irrelevant IgG [right, anti-TNFα IgG1]) staining of pure bacterial strains (two independent experiments).

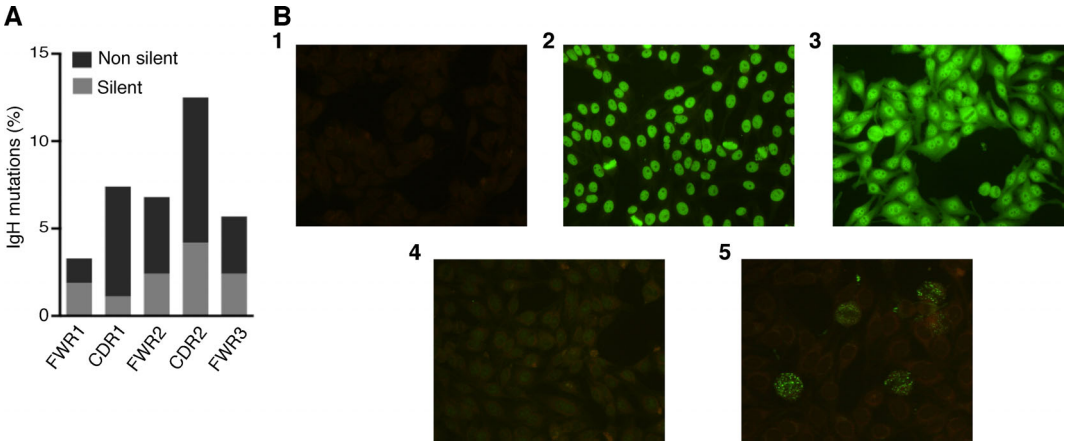

Figure S5. **Self-reactivity and glycan reactivity of antigen-selected secretory IgA. (A)** Median frequency of nonsilent (black) and silent (gray) somatic mutations in CDRs and VH FWRs in mAb *IGH* genes (n = 16 mAbs, four independent experiments). **(B)** Self-reactivity was tested by IFA with HEp-2000 cells: (1) negative control; (2) positive control: autoimmune human serum containing anti-DNA; (3) purified IgA from fecal water (20 µg/ml); (4) negative staining representative of 15 nonreactive mAbs; and (5) mAb 4. Representative images of three independent experiments are shown.

Tables S1–S3 are provided online as separate Excel files. Table S1 lists Ig gene analysis of dimeric monoclonal antibodies. Table S2 contains the demographic data of human samples. Table S3 lists primers for Ig and 16s rDNA gene sequence analysis.